Virtual Retina: A biological retina model and simulator, with contrast gain control

Adrien Wohrer · Pierre Kornprobst

Abstract We propose a new retina simulation software, called *Virtual Retina*, which transforms a video into spike trains. Our goal is twofold: Allow large scale simulations (up to 100,000 neurons) in reasonable processing times and keep a strong biological plausibility, taking into account implementation constraints. The underlying model includes a linear model of filtering in the Outer Plexiform Layer, a shunting feedback at the level of bipolar cells accounting for rapid contrast gain control, and a spike generation process modeling ganglion cells. We prove the pertinence of our software by reproducing several experimental measurements from single ganglion cells such as cat X and Y cells. This software will be an evolutionary tool for neuroscientists that need realistic large-scale input spike trains in subsequent treatments, and for educational purposes.

Keywords Large-scale retina simulator ·
Contrast gain control · Spikes · Conductances

1 Introduction

The simulator *Virtual Retina*[1] is fully documented and downloadable.[2] As an alternative solution to down-

loading, the software homepage also includes a web service[3] which allows clients to use the simulator online, through a user-friendly interface requiring no installation.

The simulator is mostly based on state-of-the-art knowledge about retinal processing, with formulations adapted to large-scale simulation. Modular XML definition files provide a simple handling of the simulator's different parameters. In this article, we detail the underlying model and the interesting features of the simulator.

Retina (and LGN) models are very numerous, ranking from detailed models of a specific physiological phenomenon, to large-scale models of the whole retina. However, interestingly, the category of large-scale models appears under-represented in retinal literature. The reason is simple: On one side, experimental researchers on the retina are not very interested in large-scale models that require mostly a compilation of already well-established results. On the other side, researchers that seek a retina/LGN input for further modeling (typically, of V1) often overlook the complexity of processing in the retina, and use very simplified retina models.

A. Wohrer · P. Kornprobst (✉)
Odyssée project team (INRIA/ENPC/ENS), INRIA,
Sophia-Antipolis, 2004 Route des Lucioles,
06902 Sophia Antipolis, France
e-mail: Pierre.Kornprobst@inria.fr

A. Wohrer
e-mail: Adrien.Wohrer@inria.fr

Our primary goal with *Virtual Retina* is to provide a better retinal input to modelers of the visual cortex. Retinal processing displays a number of features which are likely fundamental for further cortical interpretation, such as band-pass filtering, gain controls, spiking synchrony, etc. (Wohrer 2008b) It is these *functional* implications of retinal processing that we wanted to retain in the simulator. This focus on functionality naturally makes *Virtual Retina* a good candidate for a second type of application: to study the nature of the retinal code itself.

By opposition, reproducing biological complexity is not our primary goal. However, because the retina is an efficient machinery, a functional model to reproduce retinal specificities must *de facto* have an architecture quite close to that of a real retina, to allow the same sort of filtering operations.

Amongst models of retinal processing as a whole, some focus on a detailed reproduction of retinal connectivity in successive layers, each layer being modeled with a full set of cellular and synaptic parameters (Hennig et al. 2002; Bálya et el. 2002). Other models take a more functional approach, built on a series of specific filtering stages, to produce a functionally efficient retinal output. In this group, another distinction can be made between models that aim at strong biological precision (van Hateren et al. 2002; Gazeres et al. 1998; Bonin et al. 2005), and models more oriented towards signal processing and computer vision (Hérault and Durette 2007; Delorme et al. 1999), with a consequent reduction of model parameters. Many functional models are strongly inspired by the linear–nonlinear (*LN*) architecture, based on three successive stages: Linear filtering on the visual stimulus, static nonlinearity and then spike generation (Chichilnisky 2001). Because of their generality and wide use, LN models have even been termed the retinal *standard model* by Carandini et al. (2005).

For *Virtual Retina*, we propose a model somewhere in-between all models cited above. It is definitely a functional model, with consequent simplifications regarding the complexity of retinal physiology. Still, it aims at a relative biological precision: This is verified by reproducing different experimental recordings on real retinal ganglion cells, including experiments not accounted for by linear models.

LN models are also a strong inspiration to our model: The first stage consists of a spatio-temporal linear filter, and we make use of static nonlinearities. However, as opposed to LN models, we also incorporate a nonlinear mechanism of contrast gain control, inspired from retinal physiology and other existing models. Further-

more, whereas LN models are generally used to experimentally fit the responses of a few ganglion cells (Chichilnisky 2001; Keat et al. 2001; Baccus and Meister 2002), we propose here a functional model suitable for large-scale simulation.

More generally, the model keeps an architecture strongly related to retinal physiology, in a desire to reproduce specific effects which are functionally important, and often discarded by large-scale models:

- *Non-separability of the center-surround filtering.* It is well-known that most ganglion cells have a *center-surround* receptive field organization which makes them more sensitive to image edges. In real retinas, the *surround* signal is transmitted with a supplementary delay of a few milliseconds. This delay is included in our software, since it yields consequent effects for the perception of uniform screens, or appearing images. A qualitative, large-scale illustration of this fact is provided in the article.

- *Contrast gain control.* This specific nonlinear dependence of retinal filtering on the mean level of contrast is modeled in an original framework, inspired by previous models, that can account simultaneously for gain controls due to the *temporal* and *spatial* structure of the stimulus. This contrast gain control model is carefully discussed, justified mathematically, and its perceptual consequences are suggested through a qualitative simulation.

- *Adaptable band-pass temporal filtering.* In the retina, some ganglion cells have a long-lasting response after apparition of a static visual stimulus (tonic cells), while others only respond by a strong and short activation wave right after stimulus onset, and return to being silent afterward (phasic cells). *Virtual Retina* accounts for both types of cells in the simplest way possible, by modifying the strength of a partially high-pass filter.

- *Spike generation mechanism.* A possible spike generation process is proposed at the output of the software, with a model derived from experimental fitting of ganglion cell outputs (Keat et al. 2001), that yields more realistic spike trains than a Poisson process.

None of the previously cited models of retinal processing displays simultaneously all these elements. Further capabilities of the software include reproduction of *Y*-type cells' spatial nonlinearity (Enroth-Cugell and Robson 1966; Enroth-Cugell and Freeman 1987) and a possible log-polar scheme modeling the large-scale organization of primate retinas.

The article is organized as follows. In Section 2, we detail the three stages of the retina model implemented by the simulator. The first stage (2.2) is a linear filter that reproduces the *center-surround* architecture arising from the interaction between light receptors and horizontal cells. The second stage (2.3) is a contrast gain control mechanism at the level of bipolar cells, driven by feedback conductances. The third stage (2.4) provides additional temporal shaping of the signal, and then a spike generation process. Based on this model, we present in Section 3 the software simulator, *Virtual Retina*, and the results that we obtain with various sequences. First, we prove the pertinence of our model by comparing its spiking output with recordings of ganglion cells in different experiments (3.2). Then, we show large-scale simulations and more qualitative results (3.3). Finally, in Section 4, we discuss the nature of the software and its underlying model (4.1), and more specifically the included contrast gain control mechanism (4.2).

2 Methods

2.1 General structure of the model

2.1.1 A layered model in three stages

Figure 1 presents the global architecture of our model. The layered architecture of a retina suggests a model made of successive continuous spatio-temporal maps that progressively transmit and transform the incoming signal. The incoming light on the retina is the luminosity profile $L(x, y, t)$ defined for every spatial point (x, y) of the retina at each time t. It can have any units in our model; for our simulations we used digitalized intensities between 0 and 255. The subsequent layers of cells are modeled as spatial continuums (no discrete cells, except the output ganglion cells), driven by specific differential equations.

The first stage of our model deals with signal processing done in the Outer Plexiform Layer (OPL). It involves the two first layers of cells in the retina: light receptors and horizontal cells. This stage is modeled as a simple spatio-temporal linear filter based on experimental recordings (Enroth-Cugell et al. 1983; Cai et al. 1997) and previous models (Mahowald and Mead 1991; Herault 1996). We detail this OPL filter in Section 2.2. When applied to the input sequence $L(x, y, t)$, the OPL filter defines a band-pass excitatory current $I_{OPL}(x, y, t)$ which is fed to bipolar cells.

The second stage of the model is an instantaneous, nonlinear contrast gain control through a variable feedback shunt conductance $g_A(x, y, t)$, applied on bipolar cells in our model. This interaction is represented by the two small arrows between bipolar cells and the 'fast adaptation' signal in Fig. 1.

The third stage models signal processing in the Inner Plexiform Layer (IPL) and ganglion cells. First, additional spatio-temporal shaping of the signal is provided, modeling some synaptic interactions in the IPL. It produces the excitatory current I_{Gang}, which is fed to our model ganglion cells. Second, ganglion cells themselves are modeled as a discrete set of noisy integrate-and-fire (nLIF) cells paving the visual field, and generating spike trains from input current I_{Gang}. The cells that we model (see Sections 3.2.1 and 4.1.2) can be either X-type (the blue arrow, representing a one-to-one connection from bipolar cells) or Y-type (the blue cone, representing a synaptic pooling of the excitatory current).

2.1.2 Dimensional reduction

Our model equivalents to bipolar cells (Section 2.3) and ganglion cells (Section 2.4) are based on the same, generic membrane equation for a point neuron:

$$c\frac{dV}{dt} = \sum_i I_i + \sum_j g_j(E_j - V). \tag{1}$$

V is the cell's membrane potential in Volts, c is the membrane capacity in Farads. Synaptic inputs (and other intrinsic membrane currents) can either be modeled as currents I_i in Amperes, or more precisely as synaptic conductances g_j in Siemens associated to reversal potentials E_j in Volts.

Since our model does not focus on physiological precision, but on the functional output of the retina on a large scale, we are solely concerned with the *temporal* evolution induced by Eq. (1). Hence the following reduction of dimensionality:

$$V \to (V - V_R)/\Delta V, \quad I \to I/(c\Delta V), \quad g \to g/c, \tag{2}$$

where c is the membrane capacity of the neuron, V_R its resting potential, and ΔV a 'typical' range of variation for the neurons' potential. Through this reduction, constant c disappears from Eq. (1), V and the E_j become dimensionless with typical values the order of unity,

Fig. 1 Schematic view of the model, inspired by the layered structure of the retina. *Three boxes* indicate the three stages of the model. Corresponding mathematical notations are indicated in the *right-hand side*. Except for the last layer (ganglion cells), successive signals are modeled as spatially continuous maps
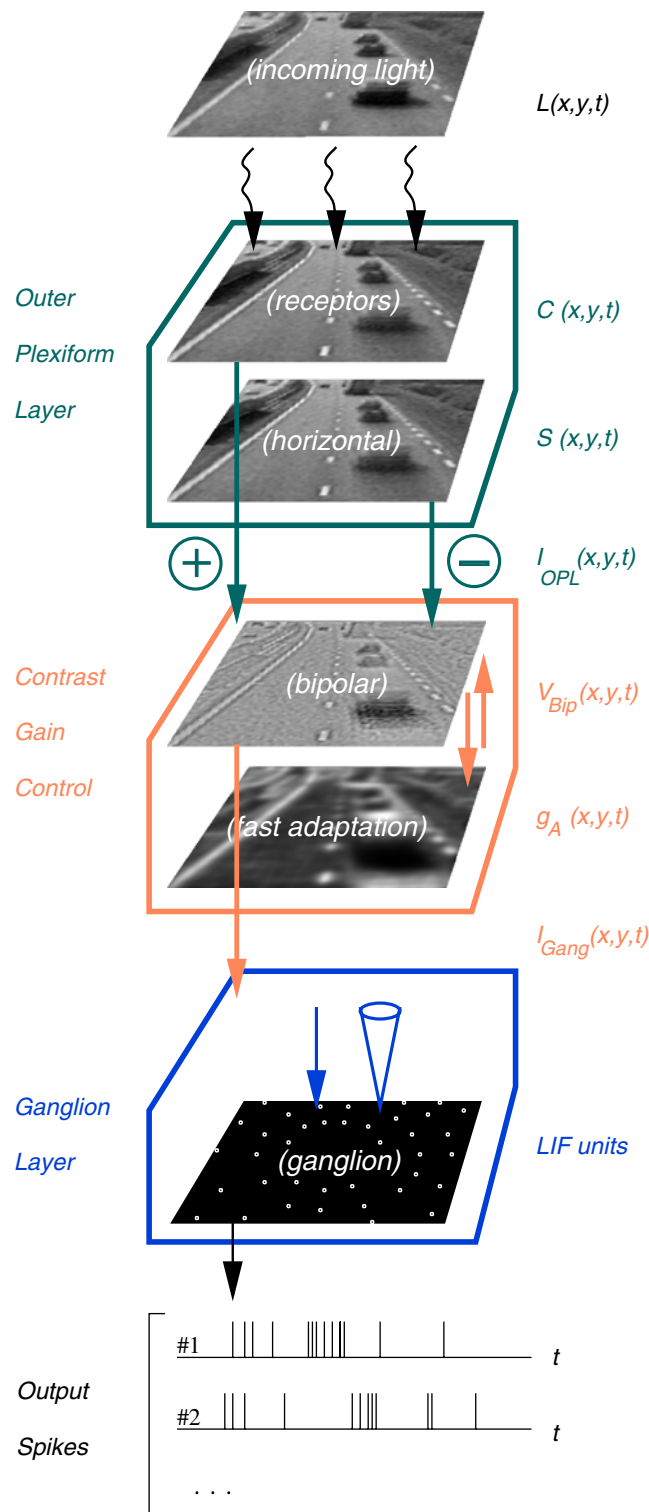
and I_i and g_j, expressed in Hertz, directly give scales for the temporal evolution of V.

Table 1 proposes a rough conversion between reduced and physical units in our model. It allows to verify that our model parameters stay in a biological range. The given conversion uses the following constants:

$$c \equiv 0.1 \text{ nF}, \quad \Delta V \equiv 20 \text{ mV}, \tag{3}$$

Table 1 Rough conversion between physical and reduced units in the model, based on Eqs. (2)–(3)

Magnitude	V (potential)	I (current)	G (conductance)
Reduced units	1 (no unit)	1 Hz	1 Hz
Physical units	20 mV	2 pA	0.1 nS

in link with physiological measurements in mammalian bipolar (Euler and Masland 2000) and ganglion (O'Brien et al. 2002) cells.

2.1.3 Notations for linear filters

As most retinal models, we use linear filters at several locations of the model, to approximate signal transformations that occur in the successive layers of the retina (see Fig. 2). This section describes the different types of linear filters used in our model. They are kept as simple as possible, because our simulator is focused on functional efficiency.

Low-pass temporal filters are taken as exponential filters, or possibly as an exponential cascade:

$$E_\tau(t) = \exp(-t/\tau)/\tau, \tag{4}$$

$$E_{n,\tau}(t) = (nt)^n \exp(-nt/\tau)/\left((n-1)!\tau^{n+1}\right), \tag{5}$$

if $t > 0$, and zero otherwise (causal filters). These are normalized filters summing to one, meaning that they are only *averaging* filters, without a linear gain. The exponential cascade filter Eq. (5) peaks at time τ (not $n\tau$), and offers more variability in the shape of the filter thanks to parameter $n > 0$.

Temporal low-pass occurs throughout retinal processing, starting at the level of photoreceptors with the complicated phototransduction cascade, and continuing in subsequent layers because of synaptic delays and membrane integration of synaptic currents.

Partially high-pass temporal filters are simply taken as the difference of a Dirac, representing the original signal, and an exponential filter representing the low-pass average removed from the original signal:

$$T_{w,\tau}(t) = \delta_0(t) - w E_\tau(t). \tag{6}$$

Temporal high-pass behavior is present in the retina with different time scales, resulting from cellular internal mechanisms (e.g. cellular adaptation), as well as from synaptic oppositions between excitatory and inhibitory cells.

Low-pass spatial filters are taken as normalized two-dimensional Gaussians:

$$G_\sigma(x, y) = \exp\left(-\left(x^2 + y^2\right)/\left(2\sigma^2\right)\right)/\left(2\pi\sigma^2\right), \tag{7}$$

which is again a normalized filter that only performs spatial *averaging* on the input signal. Gaussian kernels

Fig. 2 Linear kernels used in the model. (**a**): Exponential kernel $E_\tau(t)$ (temporal, low-pass). (**b**): Gamma (exponential cascade) kernel $E_{n,\tau}(t)$ (temporal, low-pass). (**c**): Partially high-pass kernel $T_{w,\tau}(t)$ (temporal, high-pass). (**d**): Gaussian kernel (spatial, low-pass)
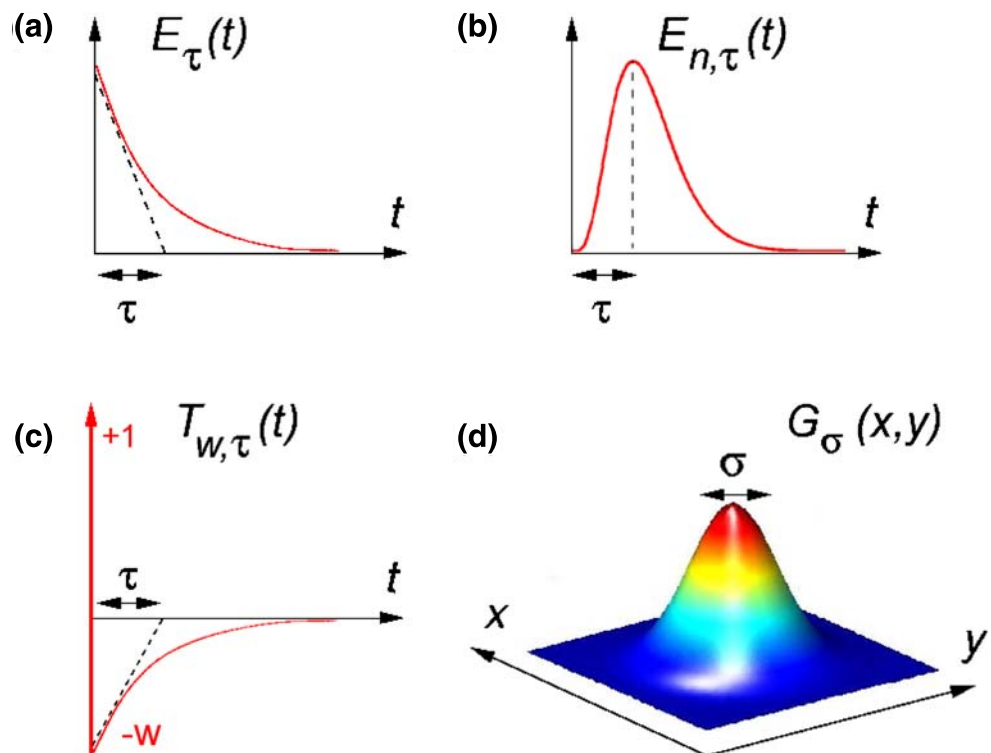
naturally arise when modeling dendritic spread of retinal cells, and also electrical couplings between cells (see Appendix A).

All filtering kernels are applied as convolution operators on their input signals. In this article, sign $\overset{t}{*}$ denotes temporal convolution, and sign $\overset{x,y}{*}$ denotes spatial convolution.

2.2 Outer plexiform layer

Retinal signals display a spatial opposition between a precise *center* signal, and a wider *surround* signal providing each location of the retina with a measure of the average illumination in the neighborhood (Barlow 1953; Kuffler 1953).

Physiologically, *OPL* is the designation for the first layer of synapses in the retina, which is the locus of synaptic interactions between light receptors, horizontal cells and bipolar cells (Masland 2001; Kolb et al. 2001). It is often assumed that the center-surround organization arises mostly in the OPL, through competing contributions from light receptors (*center*, or *C*) and horizontal cells (*surround*, or *S*) onto bipolar cells. Indeed, there is experimental evidence that a center-surround opposition is already present at the level of bipolar cells, in non-mammalian retinas (Werblin and Dowling 1969) as well as in primate retina (Dacey et al. 2000).

In our model, the resulting current $I_{OPL}(x, y, t)$ received by bipolar cells from light receptors and horizontal cells is obtained as

$$C(x, y, t) = G_{\sigma_C} \overset{x,y}{*} T_{w_U, \tau_U} \overset{t}{*} E_{n_C, \tau_C} \overset{t}{*} L(x, y, t), \quad (8)$$

$$S(x, y, t) = G_{\sigma_S} \overset{x,y}{*} E_{\tau_S} \overset{t}{*} C(x, y, t), \quad (9)$$

$$I_{OPL}(x, y, t) = \lambda_{OPL}\big(C(x, y, t) - w_{OPL}S(x, y, t)\big), \quad (10)$$

where successive convolutions are applied from right to left. $L(x, y, t)$ is the input luminosity profile. $C(x, y, t)$ represents the *center* signal, associated to light receptors, and $S(x, y, t)$ the *surround* signal, associated to horizontal cells. The linear filter resulting from Eqs. (8)–(10) is formally close to the linear approximation measured for LGN cells by Cai et al. (1997).[4] Let us comment these three equations.

---

[4]Naturally, we do not claim here that all processing up to LGN is already done in the OPL! But functionally, the linear structure of our model is mostly encompassed in this first stage, plus the supplementary linear transient $T_{w_G, \tau_G}(t)$ in Eq. (14).

Center signal [Eq. (8)]. Temporally, the phototransduction process is modeled as a partially transient linear cascade: the exponential cascade $E_{n_C, \tau_C}(t)$ is modulated by a partially transient filter $T_{w_U, \tau_U}(t)$ (*U* standing for 'undershoot'). Such filter provides an impulse response close to that measured by Schnapf et al in macaque cone receptors (Schnapf et al. 1990). Spatially, $G_{\sigma_C}(x, y)$ encompasses the spatial blur due to gap junctions between light receptors (Raviola and Gilula 1973).

Remark: nonlinearities inherent to phototransduction. The phototransduction process is in fact hardly linear, since it displays fast and slow adaptation to the ambient level of luminosity, mediated by different nonlinear processes (Schnapf et al. 1990; Valeton and Van Norren 1983; Polans et al. 1996). The linear approximation is used here for simplicity. It is relatively valid as soon as the luminosity range of the input image remains constant (Schnapf et al. 1990): room with artificial light, monitor screen... For this reason, our simulator should rather take normalized sequences as input, such as movies coded between 0 and 255.

Also, phototransduction is the only place where our software uses an exponential cascade Eq. (5), because a simple exponential approximation Eq. (4) would appear too crude.

Surround signal [Eq. (9)]. The *surround* signal is obtained through a supplementary low-pass on the *center* signal. Indeed, horizontal cells receive their input from light receptors, so their signal develops with one more synapse and one more cellular integration than receptors. Spatially, horizontal cells are very low-pass (meaning big σ_S) because of strongly coupling gap junctions with their neighboring horizontal cells (Naka and Rushton 1967; Masland 2001; Kolb et al. 2001).

OPL signal [Eq. (10)]. Constant λ_{OPL} is the overall gain of the center-surround filter, expressed in Hertz per unit of luminance. Constant $w_{OPL} \in [0, 1]$ is the relative weight of *center* and *surround* signals, physiologically measured close to 1 in mammalian ganglion cells (Enroth-Cugell and Robson 1966) and bipolar cells (Dacey et al. 2000).

Spatially, the center-surround filter Eqs. (8)–(10) can be associated to a classical difference of Gaussians (DOG). Temporally, it is biphasic. As a result, our OPL filter acts at the same time as an edge detector and a movement detector.

However, note that the center-surround filter is not *separable* in time and space: It cannot be written as

the product of a spatial kernel by a temporal kernel. Indeed, the *surround* signal is more delayed than the *center* signal because of $E_{\tau_s}(t)$ in Eq. (9).

This delay, although estimated to only a few milliseconds in mammalian retinas (Enroth-Cugell et al. 1983; Bernadete and Kaplan 1999), has significant perceptual consequences. As a result, the center-surround filter is able to detect temporal variations of luminosity even in a spatially uniform zone. This would not be the case for a separable filter, like a spatial DOG multiplied by a temporal difference-of-Exponentials. Indeed, the response of such a separable filter on a uniform region would *always* be zero because of the DOG properties, even if the luminosity does vary in time.

Also, the delay between *center* and *surround* probably implies that the first retinal spikes after onset of a new image do not code for image edges, but simply for the luminosity signal (as illustrated in Section 3.3.2).

Remark: Surround inhibition from the IPL. Specific studies suggest that some amacrine cells in the IPL also contribute to generate the *surround* component of retinal output. However, the importance of this contribution is not well established: According to the species and experimental procedure, synaptic connections in the IPL have been found to form a minority (McMahon et al. 2004), moderate (Flores-Herr et al. 2001) or important (Roska and Werblin 2001; Jacobs and Werblin 1998) contribution to ganglion cells' *surround*. Our model, aiming at functionality, neglects this additional contribution of the IPL.

2.3 Contrast gain control

Contrast gain control is the usual term to describe the influence of the local contrast of the scene on the transfer properties of the retina (Shapley and Victor 1978; Victor 1987; Kim and Rieke 2001; Rieke 2001; Baccus and Meister 2002). Consequently, it is an effect intrinsically nonlinear, and dynamical. Our simulator includes a model of contrast gain control based on

a nonlinear feedback loop at the level of our model bipolar cells:

$$\frac{dV_{\mathrm{Bip}}}{dt}(x, y, t) = I_{\mathrm{OPL}}(x, y, t) - g_{\mathrm{A}}(x, y, t) V_{\mathrm{Bip}}(x, y, t) \tag{11}$$

$$g_{\mathrm{A}}(x, y, t) = G_{\sigma_{\mathrm{A}}} \overset{x,y}{*} E_{\tau_{\mathrm{A}}} \overset{t}{*} Q(V_{\mathrm{Bip}}) \ (x, y, t), \tag{12}$$

$$Q(V_{\mathrm{Bip}}) = g_{\mathrm{A}}^0 + \lambda_{\mathrm{A}} V_{\mathrm{Bip}}^2, \tag{13}$$

where g_{A} represents a variable leakage ('shunt') term in the membranes of our model bipolar cells, which is activated through the static function Q (Fig. 3(a)). All physiological magnitudes are reduced dimensionally, as detailed in Eq. (2).

Since the leakage determines the *gain* of current integration, g_{A} has a divisive effect on the evolution of V_{Bip} in Eq. (11). At the same time, g_{A} defines the 'time constant' (not constant, here) of Eq. (11). In our model, g_{A} depends dynamically on the recent values taken by bipolar cells (feedback mechanism), with a typical time scale τ_{A} and spatial extent σ_{A}, as described by Eq. (12). These two parameters determine the size of the spatio-temporal neighborhood used by g_{A} to determine a local measure of contrast.

The possible values and biological origin of parameters σ_{A} and τ_{A} are discussed in Section 4.2. They cannot be directly fixed from experimental data, due to the hypothetical nature of the stage Eqs. (11)–(13). In the experiments of Section 3, best reproduction was obtained for a small adaptation time constant (typically, $\tau_{\mathrm{A}} = 5$ ms). As for parameter σ_{A}, we make no assumption on its possible values: it could be absent ($\sigma_{\mathrm{A}} = 0$), or present with the typical spatial extent of diffusion processes in the retina (e.g. through gap junctions) (see Discussion). Both cases are considered on a perceptual level in Section 3.3.2.

A static activation function $Q(V_{\mathrm{Bip}})$ links values of V_{Bip} to the activation of leak conductances g_{A}, through Eq. (13). Q is defined as an even function, so that the activation of g_{A} depends only on the absolute value of V_{Bip}. Parameter g_{A}^0 in Eq. (13) represents the inert

Fig. 3 Transmission functions of the model. (**a**): Activation function $Q(V_{\mathrm{Bip}})$ for shunt conductances g_{A} in bipolar cells. (**b**): Synaptic transmission $N(V_{\mathrm{Bip}})$ from bipolar to ganglion cells
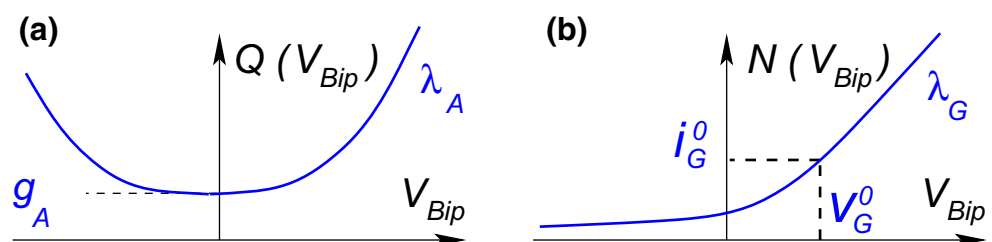
leaks in membrane integration Eq. (11) (because filters G_{σ_A} and E_{τ_A} in Eq. (12) have a gain of 1). It does not depend on the mean level of V_{Bip}. On the contrary, λ_A in Eq. (13), also in Hertz, fixes the strength of the gain control feedback loop.

Furthermore, Q is assumed to have a *convex* shape, implying different behaviors of the system, depending on the contrast:

- At small contrasts, the system has a quasi-linear working range. Indeed, when the input current I_{OPL} has small variations, it translates into small variations of the bipolar potential, so that V_{Bip} remains in the 'central region' of function Q, where $V_{Bip}^2 \simeq 0$. As a result, g_A^0 remains the principal, constant, leaking force in Eq. (11), and integration remains quasi-linear at the level of bipolar cells.
- At high contrasts, by opposition, as $|V_{Bip}|$ enters the 'big value' range of function Q, the leakage term g_A in Eq. (11) becomes truly subject to dynamical variations. As a result, bipolar cells start responding sub-linearly to the input current I_{OPL}.

Note that the precise choice of function $Q(V_{Bip})$ is arbitrary in our model (a linear-by-parts version was successively tested, but required an extra parameter, see Section 4.2). The only important constraint for our model to reproduce experimental curves, was that function Q be *strictly convex*, in order to enhance the contrast gain control effect (see Section 3.2.2).

Although the gain control mechanism proposed here is close to existing models of gain control in the retina (Victor 1987), it is an original contribution, and it is justified mathematically (see Appendix B and Wohrer 2007 for more details). We refer to Section 4.2 for comparisons between this model and previous ones. In that section we will also discuss the biological relevance of the architecture, with questions such as the symmetric shape of Q, the choice of a simple *leak* conductance, and values given to σ_A and τ_A.

2.4 Ganglion layer

The last stage of our simulator is the generation of spike trains, modeling how retinal ganglion cells produce spikes from bipolar cells' activities. First, bipolar signal V_{Bip} is rectified, and possibly receives additional spatio-temporal shaping, to produce an excitatory current on ganglion cells I_{Gang} (Section 2.4.1). From $I_{Gang}(x, y, t)$, an array of noisy leaky-integrate-and-fire neurons (nLIF), modeling ganglion cells, produces the sets of output spikes. The nLIF procedure is described in Section 2.4.2, while Section 2.4.3 shows how to define a whole retina as an assembly of nLIF. Two possible retinal organizations are discussed, log-polar or homogeneous.

2.4.1 Synaptic current upon ganglion cells

In real retinas, additional and complex transformations of the signal are provided by the synaptic structures in the *IPL*, the second layer of synapses in the retina which is the locus of synaptic interactions between bipolar cells, amacrine cells, and ganglion cells. Our simulator uses a single, empirical formula to model signal shaping in the transition from bipolar cells to classical center-surround ganglion cells (cat X and Y cells, primate parvo- and magnocellular cells):

$$I_{Gang}(x, y, t) = G_{\sigma_G} \overset{x,y}{*} N\big(\varepsilon\, T_{w_G, \tau_G} \overset{t}{*} V_{Bip}(x, y, t)\big), \quad (14)$$

with

$$N(V) = \begin{cases} \dfrac{i_G^0}{1 - \lambda_G(V - v_G^0)/i_G^0} & \text{if } V < v_G^0, \\[2ex] i_G^0 + \lambda_G(V - v_G^0) & \text{if } V > v_G^0. \end{cases} \quad (15)$$

Equations (14)–(15) do not aim to explain the biological complexity of the IPL, but to allow functional reproduction of some ganglion cells' specific responses. Parameters in these formulas will vary according to the subtype of ganglion cell being modeled. Equations (14)–(15) comprise four modeling elements:

Polarity 'ON' and 'OFF' ganglion cells are simulated simply by the simulator, by setting parameter ε in (14) to respective value 1 or -1.

Biologically, 'ON' and 'OFF' cellular pathways diverge earlier in retinal processing, involving different types of bipolar cells. From the level of bipolar cells and on, there are physiological and anatomical disparities between 'OFF' and 'ON' cells, such as reaction time, sensitivity to contrast gain control, or density of cells. These discrepancies are not explicitly taken into account by our model that considers a single, symmetrical signal up to bipolar cells. However, model parameters allow to reproduce either population, when required.

Rectification Equation (14) rectifies signal V_{Bip} through the static nonlinear function N, defined in Eq. (15) and represented in Fig. 3(b). Parameters λ_G and i_G^0 have, again, the dimension of 'reduced currents' expressed in Hertz. v_G^0 is the 'linearity threshold' of the cell, i.e. the value after which transmission becomes linear. Note that $N(v_G^0) = i_G^0$.

Such rectification is a very common feature in neural modeling and in retinal models (Carandini et al. 2005; Chichilnisky 2001; Gazeres et al. 1998). It reflects static

nonlinearities observed experimentally in the retina (Chichilnisky 2001; Kim and Rieke 2001; Baccus and Meister 2002), e.g., through *LN* analysis of retinal cells (see Section 3.2.3 for the definition of *LN* analysis). Biologically, static nonlinearities in signal transmission can occur for different reasons: saturations, synaptic transmissions, etc. Eq. (15) defines a *smooth* rectification with a shape close to experimental curves observed when performing an *LN* Analysis (see Section 3.2.3).

Additional transient The temporal filter T_{w_G, τ_G} allows to control how much the simulated ganglion cells are *phasic* or *tonic*. The tonic-phasic opposition is a general concept in physiology that can be described in simple words: *"A tonic process is one that continues for some time or indefinitely after being initiated, while a phasic process is one that shuts down quickly"* (Erwin 2004). For primate Magnocellular cells or cat Y cells, response to a constant stimulation shuts down quickly after one or two hundreds of milliseconds, requiring the use of a transient weight w_G close to 1. By opposition, for our simulations of cat X cells, the supplementary transient was fixed at an intermediate balance ($w_G = 0.7$) in order to reproduce correct Wiener kernels in Section 3.2.2, and correct responses to gratings in 3.2.1.

There are several plausible biological explanations for the transient properties intrinsic to ganglion cells. Likely, one main reason is the existence of specific amacrine cells in the IPL that were found to cut the responses of ganglion cells (Nirenberg and Meister 1997; Masland 2001; Kolb et al. 2001), whether through a feedback to bipolar cells, whether by direct inhibition on ganglion cells.

Locating this transient *before* the static nonlinearity N is a convenient, empirical choice. First, it provides better reproduction of Y cells' spatial nonlinearity (see next paragraph and Section 3.2.1) by creating fully band-pass units before the rectification and pooling. Second, it allows undershoots possibly generated by the transient filter T_{w_G, τ_G} to be attenuated by the compression N.

Additional pooling The spatial filter G_{σ_G} aims at reproducing a typical nonlinear effect observed in cat Y cells (Enroth-Cugell and Robson 1966) (an illustration can be seen in our simulations of Section 3.2.1). The simplest explanation of this spatial nonlinearity is a spatial pooling that would occur *after* the synaptic rectification onto these ganglion cells. This explanation, first proposed by Hochstein and Shapley (1976), is at the base of the Freeman and Enroth-Cugell model for Y-type cells (Enroth-Cugell and Freeman 1987). Furthermore, the biological basis was justified experimentally

(Demb et al. 2001; Kolb et al. 2001): The spread of the dendritic tree of Y-type cells is large enough to significantly average the synaptic input from bipolar cells over a consequent spatial extent.

Remark: Other explanations have been proposed to account for the nonlinearity of Y cells. For example, Hennig et al. (2002) find that part of the nonlinearity might be due to the spatial integration by Y cells of a temporal nonlinearity due to phototransduction. Although they propose a different model, their work also needs a wide spatial pooling at the level of Y cells.

2.4.2 Spike generation in ganglion cells

This section is about the transformation of the continuous signal $I_{Gang}(x, y, t)$ into discrete sets of spike trains. Let us consider N ganglion cells C_n ($n = 1 \ldots N$) paving the retinal space (see Section 2.4.3 for their repartition and parameters) and let us denote by V_n the potential of cell number n ($n = 1 \ldots N$) centered at position (x_n, y_n).

Our simulator simply generates the output of cell C_n with a standard nLIF model:

$$
\begin{cases}
\dfrac{dV_n}{dt} = I_{Gang}(x_n, y_n, t) - g^L V_n(t) + \eta_v(t), & (16) \\[2mm]
\text{Spike when threshold is reached: } V_n(t_{spk}) = 1, \\[2mm]
\text{Refractory period: } V_n(t) = 0 \text{ while } t < t_{spk} + \eta_{refr}, \\[2mm]
\text{and (16) again,}
\end{cases}
$$

where $\eta_v(t)$ and η_{refr} are two noise sources that can be added to the spike generation process in order to reproduce the trial-to-trial variability of real ganglion cells, following the experimental results of Keat et al. (2001). $\eta_v(t)$ is taken as a Brownian movement that has the dimension of a current. Integration of this current through Eq. (16) is equivalent to adding to $V_n(t)$ a Gaussian auto-correlated process with time constant $1/g^L$ (typically, 20 ms), and variance σ_v. The amplitude of $\eta_v(t)$ is chosen for σ_v to be around 0.1. η_{refr} is a stochastic absolute refractory period that is randomly chosen after each spike, following a normal law, typically $\mathcal{N}(3\,\text{ms}, 1\,\text{ms})$.

Note that spike generation is the only source of noise in our model, following the model of (Keat et al. 2001) for trial-to-trial variability in ganglion spike trains. Recent findings (Dhingra and Smith 2004) have

confirmed that the spiking mechanism is an important contribution to the overall noise in retinal processing.

Remark: ISI distributions – Poisson or not Poisson? Measuring inter-spike intervals (ISIs) is a common way of estimating the nature of the spike generation process. In real experiments, it is observed that retinal spike trains have less variability than a simple Poisson emission process (see e.g. Kara et al. 2000 for references), at least during the periods of high firing activity (Hartveit and Heggelund 1994). The coefficient of variation of retinal spike trains (CV, defined as the ratio between standard deviation and mean of the ISI histogram) was generally measured smaller than one, meaning less variability than a Poisson process. As a result, the spiking procedure has often been modeled through Gamma renewal processes, which can be seen as a generalization of Poisson processes, but with a controllable CV (see e.g. Gazeres 1998 for references).

However, in Poisson as in Gamma processes, the CV is constant whatever the input current. By opposition, some studies (Hartveit and Heggelund 1994) find that the CV of retinal spike trains depends on the intensity of the spike emission: retinal spikes become more predictable (CV decreases) during periods of high spiking activity. To account for this reality, Gazeres et al. (1998) propose a model which switches dynamically between a Poisson and a Gamma procedure with smaller CV, according to the values of the generating signal. But precise fitting of this model to biological data has not been done to our knowledge.

By comparison, the nLIF model that we use here was experimentally proved to successfully predict the occurrences of retinal spikes, in different species (Keat et al. 2001), yielding typical noise parameters that we could use in our model. An nLIF model has also been used to reproduce spike variability in the LGN (Lesica and Stanley 2004). The simulated ISIs in our nLIF model resemble those of a Gamma process, with a CV dependent on the amount of noise added in the spike generation through noise sources η_v and η_{refr} (personal experimentation).

However, we have not yet well established the behavior of the CV with input current for this nLIF model. From first experimentation, the CVs display some variability with input current (unlike a Gamma process), but not sufficiently compared to real cells. And, indeed, some experimental reproductions by our simulator suggested that our emitted spikes are probably too deterministic at low contrast. The spiking nLIF model may be enhanced in the future by adding a dynamical variation on the intensity of η_v, depending on the instantaneous intensity of the generating current.

Remark: Spike correlations between neighboring cells. Other experiments revealed a stimulus-dependent synchrony between the spikes of neighboring cells (Neuenschwander and Singer 1996) (also, see Kenyon et al. 2004; Kenyon and Marshak 1998 for a model of this synchrony based on feedbacks from long- and short-range amacrine cells). Such input-driven synchrony is not taken into account yet by the simulator, but we consider it as an interesting future extension.

2.4.3 Ganglion cell sampling configurations

The whole model presented above holds when modeling a small region of the retina, in which the density of retinal cells can be considered uniform. In that case, all filtering scales and parameters are constant and do not depend on the spatial position of each cell. Our simulation software can easily handle such a uniform distribution of cells.

However, mammalian (and especially primate) retinas taken as a whole are not uniform at all. Density of cells and filtering scales depend on the position considered in the retina. One needs to distinguish the *fovea* in the center, from the surround of the visual field where precision is less. A simple way is to define a scaling function, that describes at the same time the local density of cells and the spatial scales of filtering in the different regions of the retina.

Our simulator implements a radial and isotropic density function that depends on the distance r from the center of the retina. We define a one-dimensional log-polar scaling function $s(r)$ as

$$s(r) = \begin{cases} 1 & \text{if } r < R_0, \\ 1/(1 + K(r - R_0)) & \text{if } r > R_0, \end{cases} \tag{17}$$

where R_0 is the size of the fovea and K is the speed of density decrease outside of the fovea. When $K = 1/R_0$, this amounts to a traditional log-polar scaling. The density of cells in a given region of the retina at eccentricity r is then given by $d_0 s(r)^2$, d_0 being the 2d-density of cells in the fovea. Conversely, all spatial filtering scales of the model presented before (σ_C, σ_S, σ_{Am}, σ_{Gang}) scale with $s(r)^{-1}$.

The choice of such a scaling function is biologically justified: Dendritic trees for primate ganglion cells have experimentally been found to scale with a positive power of r, between $r^{0.7}$ and r according to the type of cell (Dacey and Petersen 1992).

3 Results

3.1 *Virtual Retina* customization

The software *Virtual Retina* implements the model presented in this article, with the following characteristics:

Possibility of large-scale simulations Up to 100,000 spiking cells can be simulated in a reasonable time (speed of around 1/100 real time).

XML definition file All parameters for the different stages of the model are defined in a single customizable XML file.

Two possible density functions First option is a uniform, square array of cells, associated to a uniform density function. In that case, all spatial filtering scales of the model (σ_C, σ_S, σ_{Am}, σ_{Gang}) are constant throughout the whole image, and the corresponding Gaussian filters $G_\sigma(x, y)$ are implemented thanks to traditional recursive Deriche filters. Second option is a sampling of ganglion cells along concentric circles, associated to the radial scaling $s(r)$ in Eq. (17). In that case, the Gaussian filters $G_\sigma(x, y)$ have different scales according to the location in the retina. They are implemented thanks to a recursive filtering with inhomogeneous recursive coefficients, an approximation proposed in Tan et al. (2003) that leads to a significant gain in computational speed.

Fixation microsaccades Finally, the software allows to include a simple random microsaccades generator at the input of the retina, to account for fixation eye movements, as inspired from Martinez-Conde et al. (2004).

To provide a better fit to the specific complexity required by potential users, we wished to build a *modular* software, that allows some liberty in the choice of the underlying model. *Virtual Retina* needs an XML file that defines all the parameters of the retina chosen for the simulation. This XML file is customizable: Each feature, as defined in this article, corresponds to its own XML node, which can be present or not in the XML definition file. One example file is shown in Appendix C.

As a result, the output of the software can consist of spikes or continuous maps, the contrast gain control can be present or not, the retina can follow a log-polar scheme or a uniform scheme, etc. This flexibility required important efforts in the conception of the software (Wohrer 2008a).

In the on-line web service, a dedicated page assists users in customizing their own XML file.

3.2 Physiological reproductions

In this section we test our simulator on classical physiological experiments, led on single ganglion cells. These experiments, with various protocols, demonstrate that our underlying model induces linear kernels close to those measured physiologically, and can also account for two typical nonlinear effects: Contrast gain control and spatial nonlinearity of Y-type ganglion cells.

A first experiment (Section 3.2.1) is devoted to reproduction of the physiological difference between X and Y- type cells. The two following experiments (Sections 3.2.2 and 3.2.3) are devoted to the phenomenon of contrast gain control in the retina. We show that our gain control loop Eqs. (11)–(13), along with the rest of the model, reproduces qualitatively the dynamical changes in retinal filtering linked to the average level of contrast.

3.2.1 X and Y cell responses to grating apparitions

Description of the experiment. Grating apparitions are a classical stimulus when experimenting on the low-level visual pathway. We reproduce here one of the first recordings of that kind, on cat ganglion cells in 1966 by Enroth-Cugell and Robson (1966), which led to the distinction between cat X type and Y type cells.

Cat 'OFF' ganglion cells are presented with the alternation of a static grating and a uniform screen of same luminance, at a frequency of about 0.5 Hz, and their spiking output is measured extracellularly. The experiment is repeated for different spatial phases of the grating, so as to test the summing properties of the cells' receptive fields. Typical responses (averaged instantaneous frequencies) for a X cell and a Y cell are presented in Fig. 4.

The experiment reveals that X cells have a relatively *tonic* behavior, since their response to a static stimulus lasts for a long time, whereas Y cells are totally *phasic*, only responding for a few hundreds of milliseconds after stimulus onset, and returning to silent.

The experiment is also an illustration of the 'null position' test: For X cells, a spatial phase exists for which the cell has roughly no response to the grating (here, 90 and 270 deg), when the 'positive' and 'negative' parts of the grating exactly compensate one another thanks to linear summation. For Y cells such a position does not exist, revealing a spatial nonlinearity, as mentioned already in Section 2.4.1.

The X cell curves in Fig. 4(a) also reveal a slow, nonlinear adaptation of the cell to its own level of response. Consider the responses of the cell at the end of the 'uniform screen' period. Linear approximation

Fig. 4 Response of cat OFF-center ganglion cells to the disappearance and reappearance of a sinusoidal grating with different spatial offsets, reproduced from Enroth-Cugell and Robson (1966). (**a**): typical X-type ganglion cell. (**b**): typical Y-type ganglion cell (see details in the text). Grating spatial frequencies of 0.13 deg^{-1} (**a**) and 0.16 deg^{-1} (**b**). Mean luminance 16 cd/m^2, grating contrast of 0.32
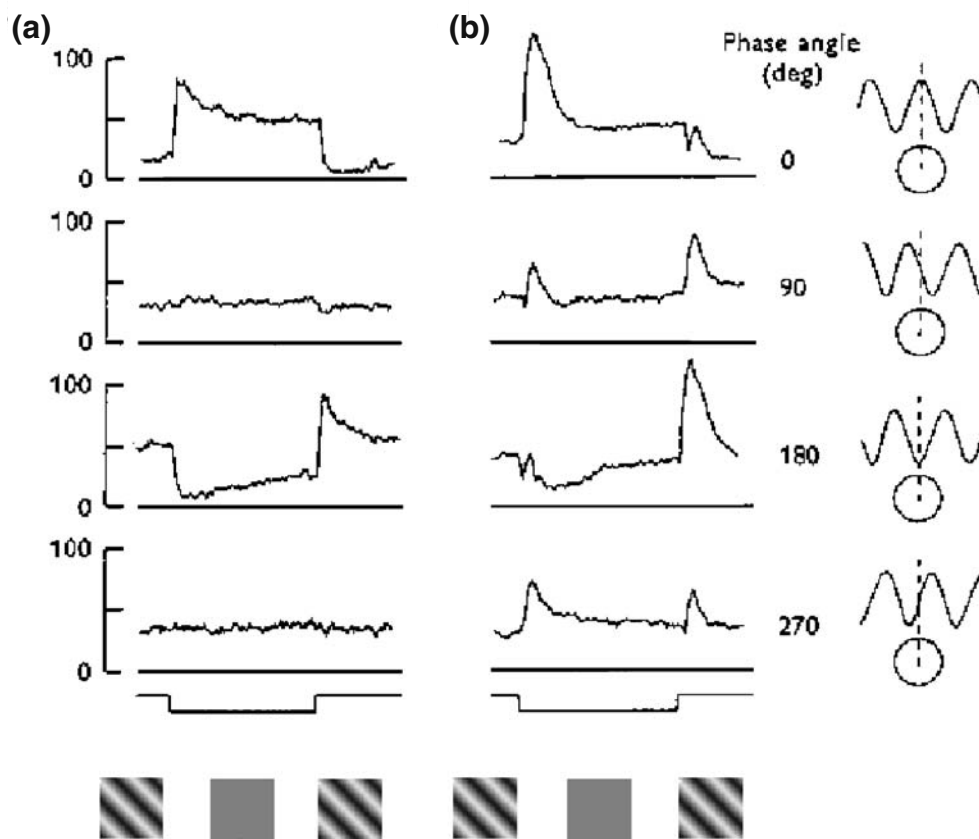
would predict similar levels of response in the four experimental conditions, since the uniform screen has already been on for a whole second, which exceeds the latency of the cell's linear response.

However, real cell responses at the end of the 'uniform screen' period are bigger in the experiment with the '0 deg' grating, and lower with the '180 deg' grating. This can be explained by a slow adaptation of the cell's gain to its global level of response, which is stronger in the '180 deg' experiment because the cell responds strongly when the grating is on.

Simulation with our model. Our modeled X and Y cells are tested in Fig. 5. Parameters σ_C and σ_S (see caption to Fig. 5) are chosen to fit the receptive fields measurements for the original X cell in Fig. 4, by the authors. Other parameters are chosen to produce a good, simultaneous fit to these experiments and the following (multi-sinus, LN analysis).

The model reproduces the 'null position' typical of X cells, and the absence of such 'null position' for Y cells, due to the post-synaptic pooling added in Eq. (14). Reproduction of Y cell curves required that the three modeling elements in Eq. (14) be in the right order: temporal transient T_{w_G, τ_G}, rectification N and pooling G_{σ_G}.

The slow decay of X cell responses to static stimuli is also reproduced, with the correct time scale. This is due to the added effects of the two transient filters in our retinal scheme: slow transients with T_{w_U, τ_U} in Eq. (10), and fast transients with T_{w_G, τ_G} in Eq. (14).

Note however that in our model, in any of the four experimental conditions, the X cell sets back to the same firing rate at the end of the 'uniform screen' period: its ground firing rate. Parameters i_G^0 in Eq. (15) and g^L in Eq. (16) were fixed to obtain a ground firing rate of around 50 Hz. Our model does not encompass the slow cellular adaptation of the cell to its own level of response, observed in Fig. 4(a) and explained in the previous paragraph. Slow adaptation is discussed in Section 4.2.

3.2.2 Multi-sinus experiments

To test and calibrate our contrast gain control loop Eqs. (11)–(13), we reproduced two of the Shapley and Victor (1978) multi-sinus experiments, which gave the first quantitative measures of contrast gain control in the retina. These experiments were pursued on an ON-center cat X cell. Input stimulus $L(x, y, t)$ was a static grating of fixed mean luminance $\bar{L} = 20$ cd/m^2,
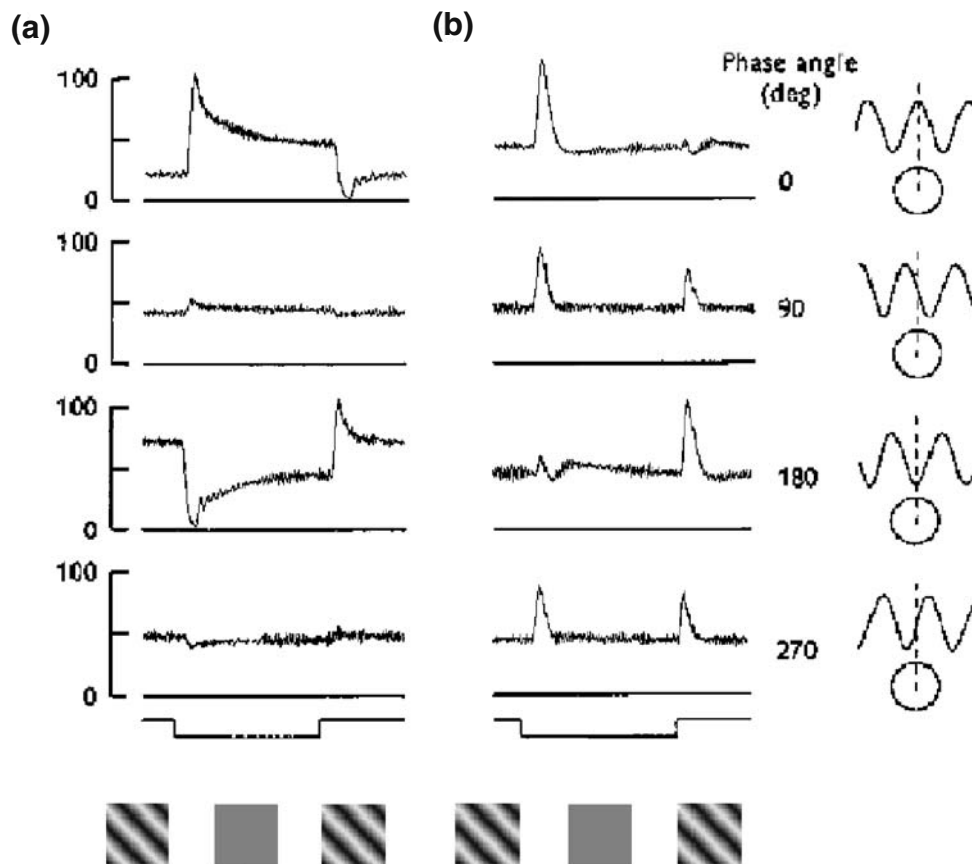
Fig. 5 Reproduction of the experiments in Fig. 4 by our retina model. (**a**:) X cell model, (**b**:) Y cell model. Average firing rates generated from 80 trials with noise in the spike generation. *Test grating:* Normalized mean luminance of 0.5, contrast 0.32, spatial frequency of 0.13 deg^{-1}. **OPL parameters:** *Center*, $\sigma_C = 0.88$ deg, $\tau_C = 10$ ms, $n_C = 2$. *Surround*, $\sigma_S = 2.35$ deg, $\tau_S = 10$ ms. *Slow linear transient*, $w_U = 0.8$, $\tau_U = 100$ ms. *Global amplification*,

$\lambda_{OPL} = 1000$ Hz per normalized luminance unit. **Gain control parameters:** $g_A^0 = 5$ Hz, $\lambda_A = 50$ Hz, $\tau_A = 5$ ms, $\sigma_A = 2.5$ deg. **X cell parameters:** *IPL transients*, $w_G = 0.7$, $\tau_G = 20$ ms. *Synaptic transmission*, $\sigma_G = 0$, $\lambda_G = 150$ Hz, $v_G^0 = 0$, $i_G^0 = 80$ Hz. **Y cell parameters:** *IPL transients*, $w_G = 1$, $\tau_G = 50$ ms. *Synaptic transmission*, $\sigma_G = 1.8$ deg, $\lambda_G = 300$ Hz, $v_G^0 = 0$, $i_G^0 = 80$ Hz. **Spike generation:** $g^L = 50$ Hz, $\sigma_v = 0.2$, $\eta_{refr} \sim \mathcal{N}(3$ ms, 1 ms$)$

temporally modulated by a sum of sinusoids with adjustable contrasts:

$$L(x, y, t) = \bar{L} \left(1 + \text{Gr}(x, y) \sum_{i=1}^{8} c_i \sin(\xi_i t) \right), \quad (18)$$

where $\text{Gr}(x, y)$ is a sinusoidal grating function with normalized amplitude (between -1 and 1). The ξ_i are a set of eight temporal frequencies that logarithmically span the frequency range from about 0.2 to 32 Hz, respectively associated to contrast strengths c_i.

Recordings were made for different distributions of the c_i. For each recording, the cell's output firing rate was Fourier-analyzed at each of the input frequencies ξ_i, thus yielding a set of eight amplitudes and eight phases. This set provided a measure for the linear kernel (first-order Wiener kernel) that best fits the cell's response, *in the given contrast conditions*.

Influence of the mean level of contrast

Description of the experiment. This first experiment measures how the mean level of contrast changes the best-fitting first-order Wiener kernel for the cell. The c_i are all fixed at the same value $c_i = c$, global level of contrast for the stimulus. The experiment is repeated for four values of contrast, c being doubled each time.

Remark When $\forall i$, $c_i = c$, the temporal part of signal Eq. (18) is related to a *pink noise* stimulus (with similar power in each frequency octave). However, the spectrum of Eq. (18) is concentrated on eight discrete values, unlike a real pink noise.

The resulting amplitude and phase diagrams for the cell's output, represented in Fig. 6(a) and (b), reveal deviations from linearity: If the ganglion cell responded

Fig. 6 Contrast gain control in a cat ON-center X ganglion cell, reproduced from Shapley and Victor (1978). (**a** and **b**): response to multi-sinus stimuli of different contrasts c (sample input signal depicted in panel **c**-*1*). Amplitude curves (**a**) reveal under-linearity at low temporal frequencies. Phase curves (**b**) reveal time advance for high contrasts (see text). Successively, c was 0.0125 (○), 0.025 (□), 0.05 (△) and 0.1 (●). (**d**): Strength of the gain control effect depends on the dominant frequency ξ_{i_0} present in the input (stimuli with a carrier frequency ξ_{i_0}, as depicted in Panel **c**-*2*). The three curves represent indicators $\phi_5(\xi_{i_0})$ (●), $\phi_6(\xi_{i_0})$ (■) and $\phi_7(\xi_{i_0})$ (▲) which measure the strength of the gain control (see text). Frequencies that elicit the most gain control are $\xi_{i_0} =$ 3–10 Hz
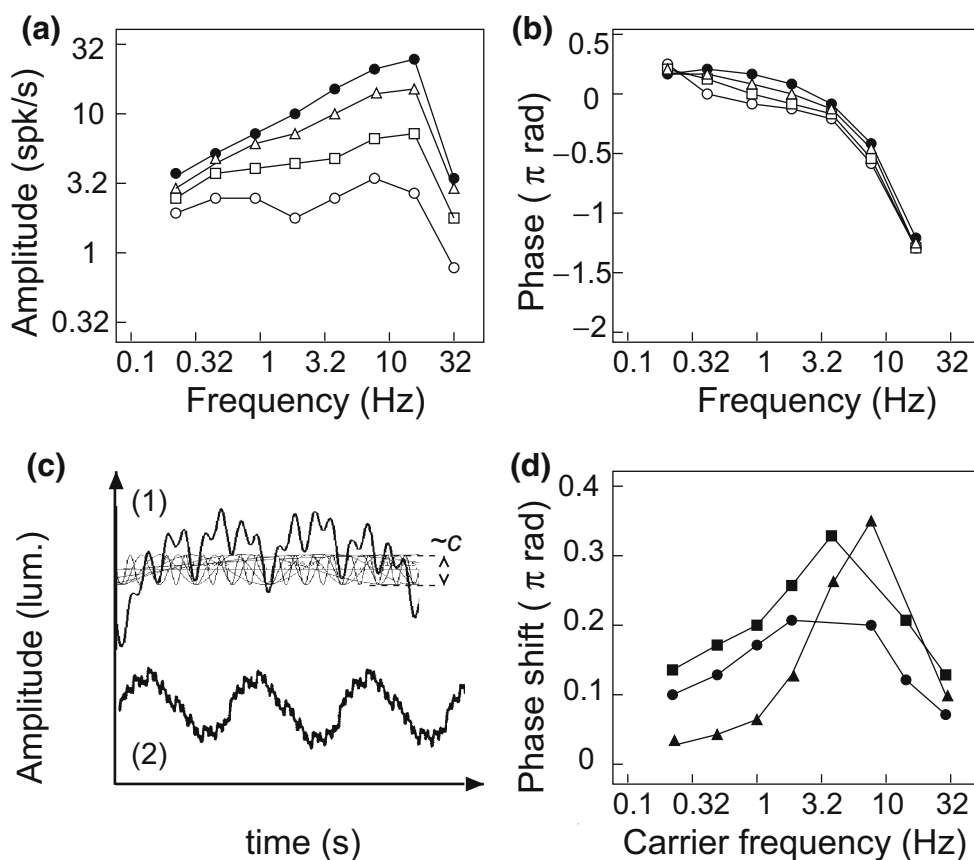
linearly to its input, the modulations in its response would simply be proportional to c. Successive amplitude curves in Fig. 6(a) would be parallel, spaced by log(2) as contrast is doubled, and all phase curves in Fig. 6(b) would superimpose, since the phase portrait depends only on the nature of the linear filter.

Instead, the cell responds under-linearly to contrast at low temporal frequencies, where successive amplitude curves are spaced by less than log(2). In the phase portrait, strong contrasts induce a phase-advance of the response (phase curve shifted upwards), meaning that the cell responds *faster* at high contrasts. Amplitude compression at low frequencies and phase advance are the dual mark of the contrast gain control effect, as defined by Shapley and Victor. The authors found the two phenomena to be highly correlated in their experiments, probably resulting from a common mechanism.

Simulation with our model Reproduction by our model is shown in Fig. 7(a) and (b). The model reproduces the typical time advance of ganglion responses at high contrasts (Fig. 7(b)). This is because conductance g_A in Eq. (11) determines the time constant of the response of bipolar cells, and that the mean level of g_A,

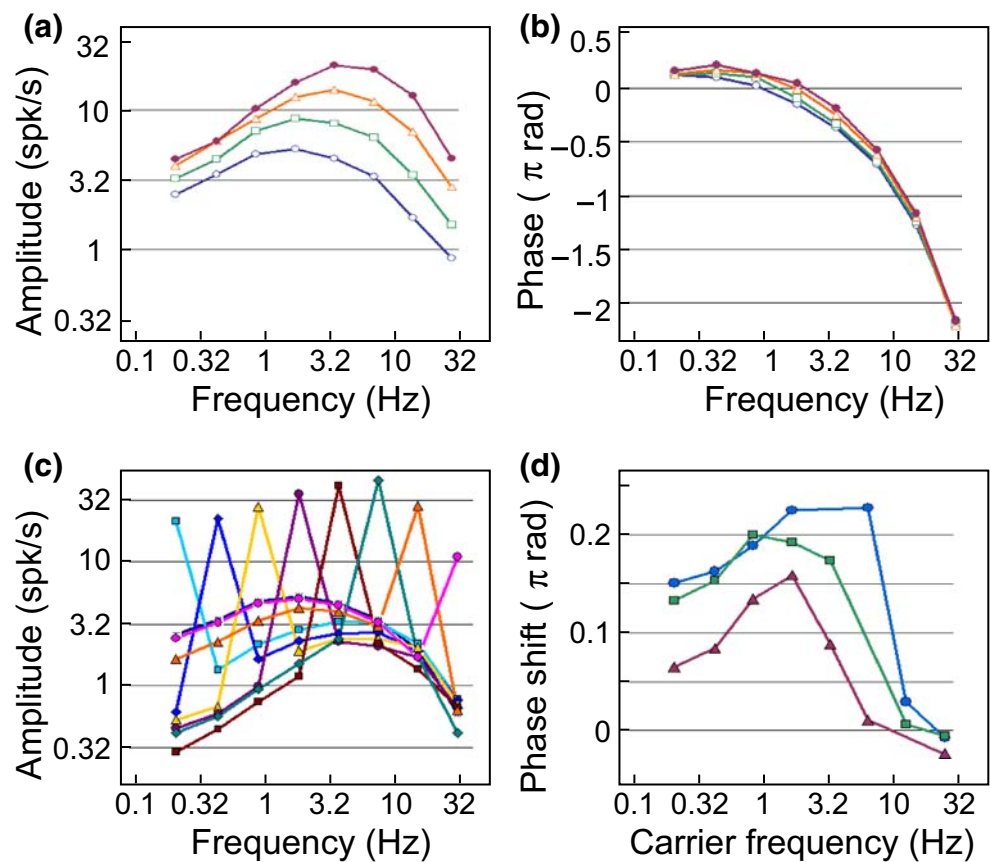dependent on the average of V_{Bip}^2, is a growing value of contrast.

Similarly, the under-linearity of response amplitudes with contrast is also observed (successive curves spaced by less than log(2) in Fig. 7(a)). This is because g_A in Eq. (11) increases the leak in the bipolar membrane, and thus lowers the linear gain of bipolar transmission in the case of high input contrast.

According to the preceding intuitive explanation, any shunting feedback loop necessarily implies a phase advance and an amplitude compression, and thus contrast gain control. However, reproducing the exact *shape* of the kernel, and how it varies with contrast, required more specific features from our model.

First, the feedback loop Eqs. (11)–(13) is globally a low-pass setting, that can by no means reproduce the band-pass behavior observed in Fig. 6(a). The band-pass behavior in our model arises *before* the feedback loop, through filter T_{w_U,τ_U} in Eq. (8) that accounts for temporal transients in the first layers of the retina, and *after* the feedback loop, through filter T_{w_G,τ_G} in Eq. (15) that accounts for temporal transients in the IPL.

Second, we found mandatory that function Q in Eq. (13) be *strictly convex* with a flat zone around $V_{\text{Bip}} = 0$, in order to reproduce the pronounced change

Fig. 7 Reproduction of the gain control effect by a model cat X cell. (**a**), (**b**) and (**d**) have same signification as in Fig. 6 (including various curve markers). (**c**) represents the amplitude responses for the model cell in the 'carrier frequency' experiments (stimuli as in Fig. 6(c-2)). Contrast gain control is observed since the 'perturbation' kernels do not superimpose (see text). *Test grating:* mean luminance of 0.5, 0.2 cycles/deg. *X Cell parameters* as in Fig. 5

Frequencies that induce contrast gain control

Description of the experiment. A second experiment was crafted by Shapley and Victor (1978) to further investigate the origin of the gain control mechanism. Each input frequency ξ_{i_0} is successively chosen as a 'carrier' frequency with $c_{i_0} = 0.2$, while the other frequencies are added as perturbation terms: $c_i = 0.0125$ for $i \neq i_0$ [see Eq. (18)]. Results are compared to a 'low contrast' test condition where $c_i = 0.0125$ for all i.

For each carrier frequency ξ_{i_0} three phase advance indicators $\phi_5(\xi_{i_0})$, $\phi_6(\xi_{i_0})$ and $\phi_7(\xi_{i_0})$ are measured, respectively associated to *assay frequencies* $\xi_5 = 3.9$, $\xi_6 = 7.8$ and $\xi_7 = 15.6$ Hz. $\phi_5(\xi_{i_0})$ is obtained by measuring output phase at the assay frequency ξ_5 when ξ_{i_0} is the carrier frequency, and subtracting the output phase at

ξ_5 in the low-contrast test condition; similarly for $\phi_6(\xi_{i_0})$ and $\phi_7(\xi_{i_0})$.

Since contrast gain control can be measured by a phase advance (previous paragraph), $\phi_5(\xi_{i_0})$, $\phi_6(\xi_{i_0})$ and $\phi_7(\xi_{i_0})$ provide three indicators, hopefully highly correlated, of the strength of the gain control induced by ξ_{i_0}.

Figure 6(d) represents experimental measures for $\phi_5(\xi_{i_0})$, $\phi_6(\xi_{i_0})$ and $\phi_7(\xi_{i_0})$. As predicted, the three indicators are highly correlated, consistently with the global time advance induced by contrast gain control. Phase advance is strongest when the carrier ξ_{i_0} is around $3 - 10$ Hz. This reveals that the underlying mechanism for the contrast gain control measured here has a 'band-pass' sensitivity, being preferentially triggered by temporal variations around $3 - 10$ Hz.

Simulation with our model. The three measured phase differences $\phi_5(\xi_{i_0})$, $\phi_6(\xi_{i_0})$ and $\phi_7(\xi_{i_0})$ for our model are represented in Fig. 7(d). We reproduce larger phase advances when the carrier frequency is in the range $1 - 10$ Hz. This is due to the temporal band-pass filter T_{w_U, τ_U} in Eq. (8), that enhances the contributions of frequencies $1 - 10$ Hz in the current I_{OPL} which is fed to the gain control mechanism Eq. (11).

Fig. 8 (**a**) and (**b**): LN analysis by Baccus and Meister (2002) on a salamander ganglion cell, revealing contrast gain control. Time advance can be observed (**a**), and decrease of the gain at high contrasts (**b**). (**c**) and (**d**): LN analysis on a model cell, based on a spike-triggered average as in Chichilnisky (2001) (time bin 5 ms). Same parameters as the model X cell in Fig. 5, except for slower time scales to account for the salamander retina: $\tau_C = 30$ ms, $\tau_S = 20$ ms, $\tau_G = 50$ ms, $i_G^0 = 0$ Hz, $\lambda_G = 300$ Hz
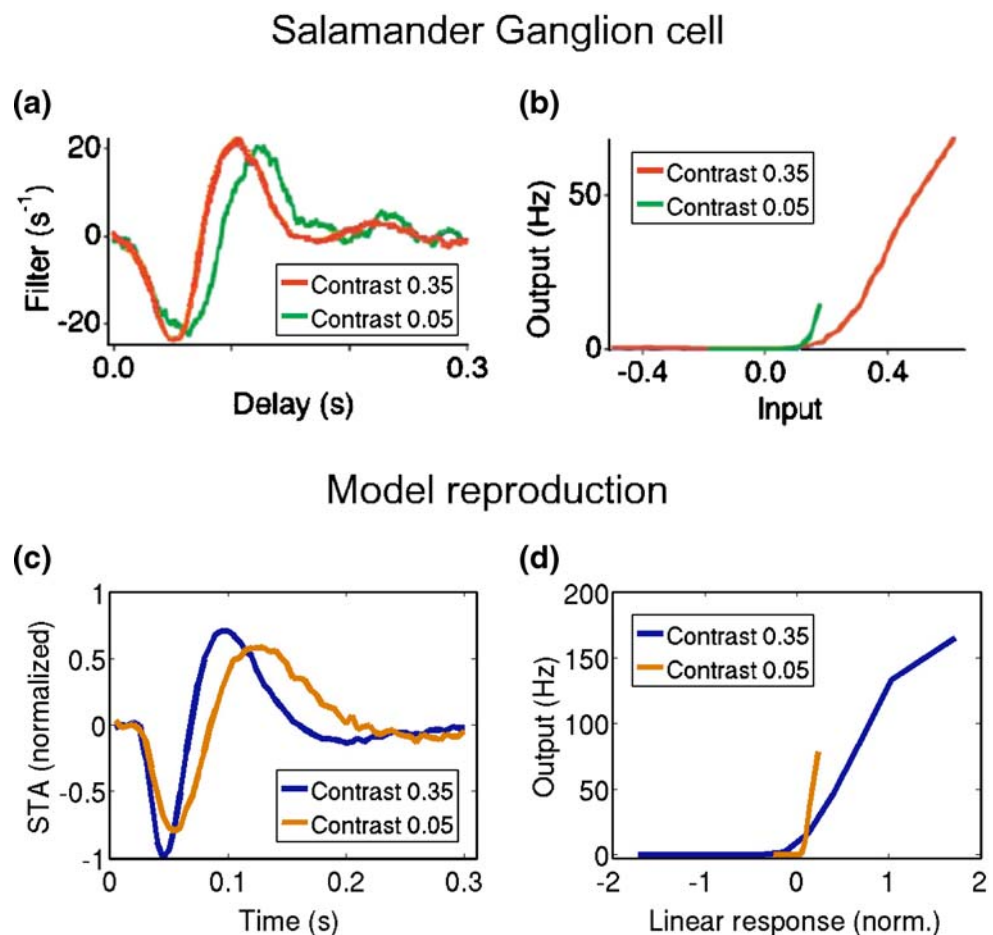
In Fig. 7(c) we also provide the Wiener kernels associated to the experiment. Given a carrier frequency ξ_{i_0}, the interesting feature is the *perturbed kernel* measured at the remaining frequencies $\xi_i \neq \xi_{i_0}$. Perturbed kernels for different carriers ξ_{i_0} do not superimpose, because all carriers do not imply the same amount of gain control. Strong gain control translates in a Wiener kernel that is more cut at low temporal frequencies. For our set of parameters, we find that the carrier frequencies that elicit the most gain control are $\xi_{i_0} = 4$, 8 and 2 Hz, coherently with Fig. 7(d).

3.2.3 Linear–nonlinear analysis (LN)

Another way to compute Wiener kernels is LN analysis, based on reverse correlation of the output signal with a white noise stimulus (Marmarelis and Naka 1972; Chichilnisky 2001). It provides a way to measure the LN architecture (linear filtering followed by a static non-linearity) that best fits the measured cell. This method has been recently applied to the retina to provide new measurements of contrast gain control (Kim and Rieke 2001; Rieke 2001; Baccus and Meister 2002).

Figure 8(a) and (b) presents experimental results of Baccus and Meister (2002) on a salamander ganglion cell. They performed an LN analysis with white noise at two different contrasts, to measure the change in the filtering structure of the cell. The dual mark of contrast gain control is again observed: time advance of the response (Fig. 8(a)) and decrease of the gain for high contrasts (slope of the nonlinear function in Fig. 8(b)).

LN analysis on a model cell is depicted in Fig. 8(c) and (d). Our simulated cell is based on the X cell model of Fig. 5, except for time scales which were fitted to salamander retina time constants. The dependence on contrast of the linear filter and nonlinear curve is qualitatively similar to the original experiment.

Remark It is not suprising that our model performs well both on this LN protocol and on the previous multi-sinus protocol (Section 3.2.2). Indeed, both protocols derive a 'best-fitting linear kernel', in response to a temporal signal which browses the whole frequency domain. However, LN analysis generally uses white noise, while the multi-sinus experiment is more related

to pink noise (preceding remark). As a result, the retrieved kernels slightly differ between the two protocols (personal experimentation).

Remark Fast and slow contrast gain control Recent work (Kim and Rieke 2001; Baccus and Meister 2002) has established that at least two contrast gain control mechanisms are present in the retina with different time scales: A fast, almost instantaneous gain control mechanism, and a slower adaptation process (see discussion in Section 4.2). The multi-sinus experiments (Shapley and Victor 1978) in Fig. 6 use a protocol which elicits both the slow and fast mechanisms. By opposition, the LN experiments of Baccus and Meister (2002) do discriminate fast from slow contrast gain control. The curves in Fig. 8(a) correspond specifically to their measure of the *fast* effect.

Our model only includes a fast gain control mechanism. Figure 8(b) shows that our mechanism can qualitatively reproduce the fast component of contrast gain control. In turn, Fig. 7 shows that our mechanism is *sufficient* to qualitatively reproduce the multi-sinus experiments, suggesting that biologically, *fast* contrast

gain control is mostly responsible for the change in shape of the kernels (a result confirmed in Baccus and Meister 2002).

3.3 Results on real images

To conclude our presentation of *Virtual Retina*, we present simulations on whole images and sequences. We do not study quantitatively any retinal feature in this section: The article does not aim at such study, but at presenting a simulation tool. Rather, we illustrate qualitatively how large-scale simulations allow to link a model architecture with its perceptual consequences.

First, as a general illustration of the software, we present the complete simulation of a retina on a moving sequence, with spiking output and all intermediate signals involved. Second, we focus on two specific elements of the model and how they relate to a percept.

3.3.1 Large-scale simulation of the model

We show in Fig. 9 the response of our model to an input video stimulation, with all intermediate signals

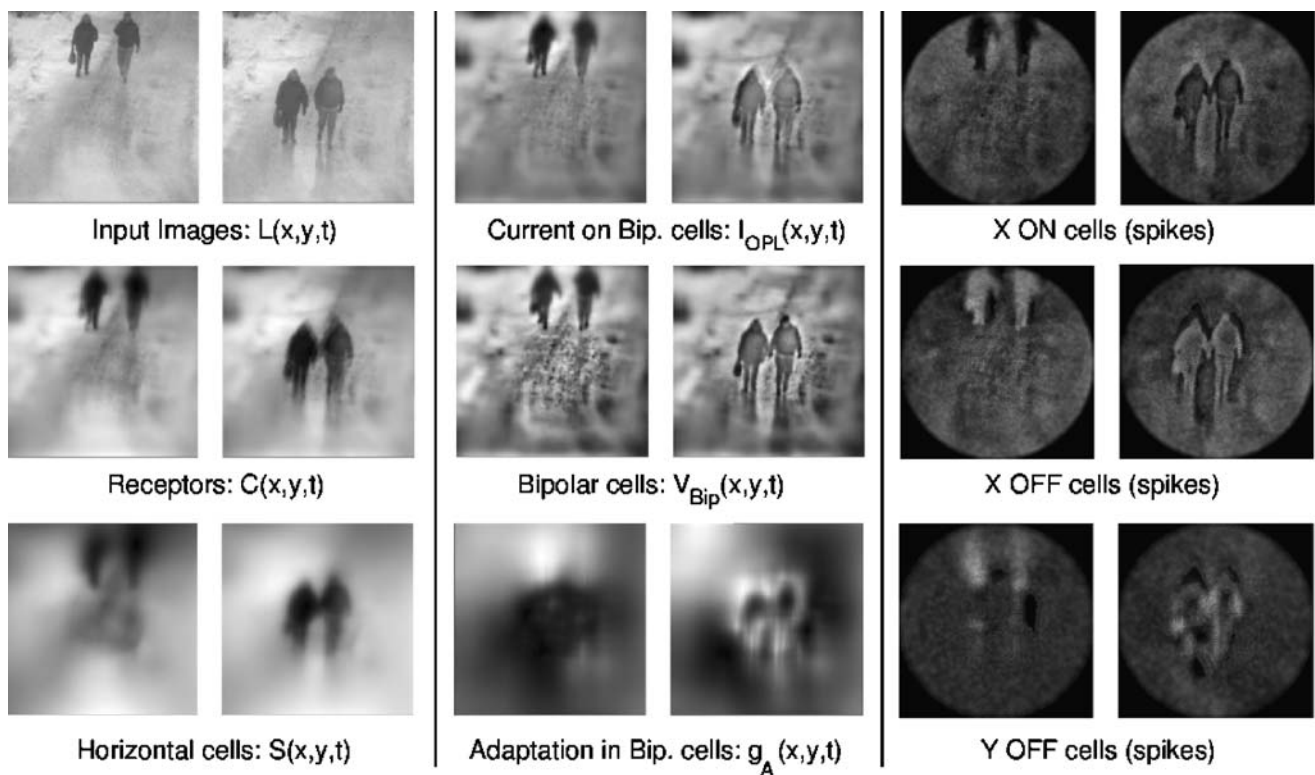
Fig. 9 Large-scale simulation with cat X and Y cells. Image size: 50 deg (250 pixels). Same parameters as in Fig. 5, except $\sigma_C = 0.3$ deg, $\sigma_S = 1$ deg, and for Y cells $\sigma_G = 1$ deg, $i_G^0 = 60$ Hz. Artificial radial structure as in primate retinas: $R_0 = 10$ deg (50 pix), $K = 0.2$ deg^{-1}. 90,000 spiking cells, simulation speed of around 1/100 real time (see text)

represented at two instants of the simulation. To display all possibilities of *Virtual Retina*, we chose a hybrid retina, with cell properties being those of a cat retina (with X and Y cells), but that displays a radial structure as in a primate retina, with spatial precision maximum in the fovea, and decreasing towards the periphery. The simulated retina had a diameter of 50 deg, corresponding to 250 pixels. The input sequence lasted 1.4 s of 'real time', corresponding to 56 frames (each frame shown for 25 ms). There were three ganglion layers of 30,000 spiking cells each. On average, each cell fired approximatively one spike per input frame. Total processing time was around 130 s (2 s per input frame).

The foveated structure, ruled by sampling scheme Eq. (17), can be observed on all retinal images (except for the input light): The periphery is more blurred than the central zone.

Signals C, S and I_{OPL} illustrate the properties of the OPL filter Eqs. (8)–(10): It is the difference of two low-passed versions of the sequence, so it takes strong values on *image edges* and on *moving zones*. Its biggest response is thus located on the edges of the walking characters.

Second column corresponds to layers I_{OPL}, V_{Bip} and g_A which are involved in the contrast gain control scheme Eqs. (11)–(13). The contrast gain control scheme enhances the linear contrast image I_{OPL} to produce V_{Bip} (which reveals better the details of contrast). This perceptual effect is detailed in the sequel.

Last column presents linear reconstructions from the output spike trains, respectively from X ON and OFF cells, and Y OFF cells. Each spike simply contributes to the reconstruction by adding a circular spot, whose diameter and intensity depend on the cell density in this region of the retina, and whose temporal profile is a decreasing exponential of time constant 20 ms. Thus, a reconstructed sequence displays in each pixel a quantity close to the 'instantaneous firing rate for a cell located at this pixel'.

The positive and negative parts of signal V_{Bip} are coded respectively by ON and OFF ganglion cells. Y cells display a signal with less spatial precision than X cells, because of the supplementary synaptic pooling G_{σ_G} in Eqs. (14). Second, Y cells are only sensitive to temporal changes, so they only detect the moving characters. This is obtained by making Y cells totally phasic with $w_G = 1$ in Eq. (14), and by lowering the spontaneous firing rate of Y cells, through parameter i_0^G in Eq. (15).

3.3.2 Perceptual consequences of model architecture

Spiking pattern at image onset

It has long been known that the *center-surround* architecture of ganglion cells produces preferential responses to spatial or temporal change. Many subsequent modeling has considered the retina – or at least its *center-surround* ganglion cells pathway – as an *edge detector*. Here we suggest there could be another effect in the first milliseconds after image onset, due to the biologically observed delay of *surround* signal w.r.t *center* signal (Enroth-Cugell et al. 1983; Bernadete and Kaplan 1999).

Figure 10 presents a reconstruction from the spikes emitted by a square array of primate 'parvo'-like cells, after onset of a static image (one cell per pixel, each spike adding an exponential contribution of latency 15 ms). To produce plausible initial conditions, the cells are previously exposed to Gaussian white noise of same luminance as the forthcoming image.

The first spikes coding for the image (observable from around 20 ms after image onset) do not code for image edges, but only for the *center* signal, simply proportional to the input luminance: see reconstruction at time 30 ms. The following spikes progressively start coding for image edges, as the delayed *surround* signal [Eq. (9)] catches up. In the reconstruction of Fig. 10, the transition is partly achieved at time 50 ms, totally achieved at time 90 ms. It is surprising, but verified, that the small supplementary delay of *surround* (here, $\tau_S = 4$ ms) has perceptual effects over several tens of milliseconds.

Very recent results (Gollisch and Meister 2008) have brought experimental validation to this original prediction of our model. The authors reconstructed two images from the spike trains of a salamander fast OFF ganglion cell in response to the onset of a static image: A first reconstruction image based on the latency of the first emitted spike (T), and a second image based on the total number of spikes fired by the cell (N). Their observation, reproduced with our model (not shown), is that the 'T' image resembles the luminance input profile, while the 'N' image puts more accent on image edges.

In our model, this subsequent 'edge image' is the *equilibrium* signal of the retina: It defines the 'stabilized' retinal output to the static image, after the initial luminance transient at image onset (in real retinas, 'stabilized' is only an approximation, due to slow adaptation effects). But the initial 'luminance transient'

Fig. 10 Spiking cells respond to the onset of a static image, after exposure to noise of similar luminance. First spikes code for a luminance signal (see reconstruction 30 ms after image onset). The 'edge detection' signal is coded only in the following spikes (see reconstruction at 90 ms), due to the non-separability of filtering in the OPL (see text). *Experimental procedure:* Primate 'parvo'-like cells: $\sigma_C = 0.03$ deg, $\sigma_S = 0.1$ deg, $\sigma_A = 0.2$ deg; $\tau_S = 4$ ms, approximative delay measured between *center* and *surround* signal in cat (Enroth-Cugell et al. 1983) and primate (Bernadete and Kaplan 1999). Other parameters as in Fig. 5. Input image 5 deg (500 pixels). Output array: 100×100 cells, one cell per pixel in the reconstruction

Original Image | 30 ms

50 ms | 90 ms
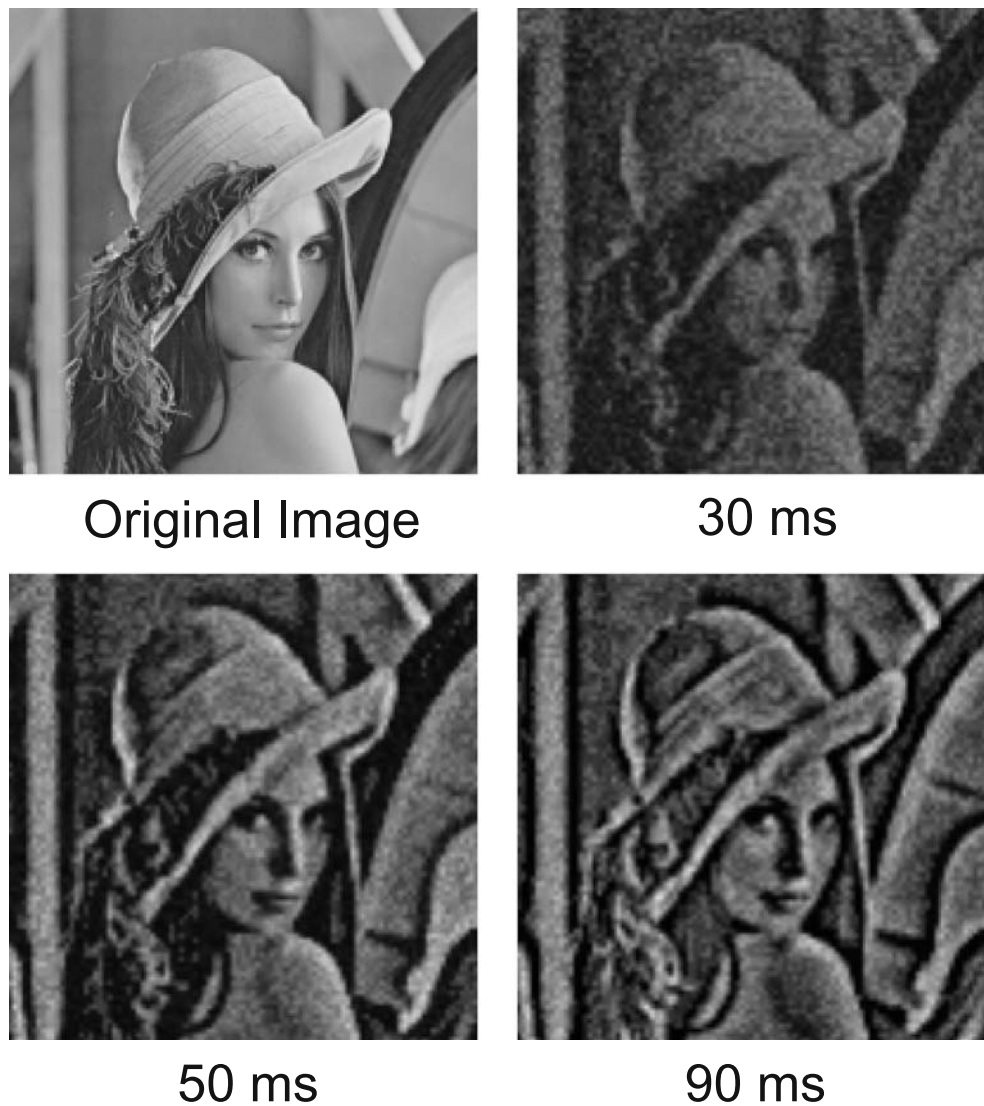
probably has its importance for studies of spike-related information transmission. If it is true that the first emitted spikes carry the most information (Berry et al. 1997; Van Rullen and Thorpe 2001), is the retina really an edge detector?

We believe that a large-scale, and relatively detailed simulator such as *Virtual Retina* can be of some help to theoreticians wishing to address this 'delayed surround' problem more quantitatively. One object of our current research is to find reconstruction procedures taking advantage of this particular structure of retinal filtering (see Conclusion).

*Remark* Using the basic microsaccade generator included in *Virtual Retina*, we also tested what signal is coded when the image is subject to small, regular displacements of frequency around 2 Hz (Martinez-Conde et al. 2004). We found that the 'microsaccade'-perturbed image remains perceptually close to the stabilized 'edge image'. This further justifies our de-nomination of the 'edge image' as being 'stabilized', even under small fixation eye movements.

Contrast enhancement through contrast gain control

As a second illustration of the relation between models and large-scale percepts, we present in Fig. 11 how the gain control loop Eqs. (11)–(13) enhances edges nonlinearly, in ways very similar to traditional image processing techniques.

The test image displays a flower with strong contrast, and smaller variations of contrast in the background.

Fig. 11 Perceptual comparison between a linear output (**b**) and two versions of the gain control mechanism. When the gain control is purely temporal (σ_A=0, panel **c**), it operates as a point-by-point Gamma transform on the image. When the gain control is allowed to have a spatial extent (**d**), it operates like a local histogram equalization on the contrast image. (**b**) to (**d**) are equilibrium responses, after the initial transient at image onset. Details and experimental procedure in the text. Flower photo courtesy of Marcello Moisan (Moisan 2007)
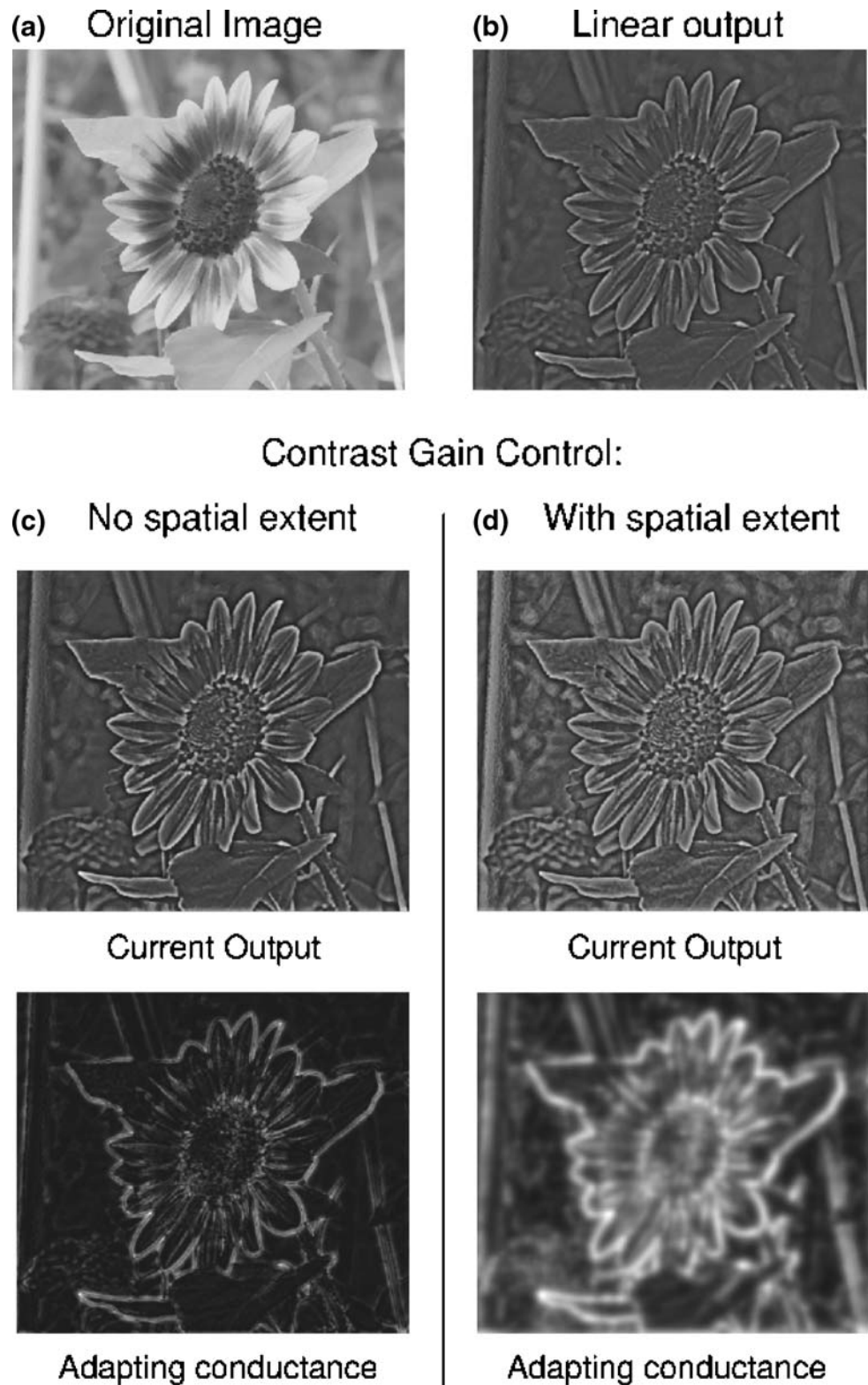
We only consider here the *equilibrium* 'edge image' of the retina, rather than the initial 'luminance transient' (as explained in the previous paragraph).

We compare the linear output of the retina I_{OPL} with two versions of V_{Bip} after contrast gain control. First version considers a purely temporal gain control

loop, with no spatial extent for the measure of contrast by $g_A(x, y, t)$ (through $\sigma_A = 0$ in Eq. (12)). A second version allows this spatial extent, with $\sigma_A = 0.2$ deg, a value comparable to the extent of our surround signal $\sigma_S = 0.1$ deg. We study these two cases distinctly because of the hypothetical nature of parameter σ_A in our retinal model (see Discussion in Section 4.2).

To produce comparable results, the three resulting images ($I_{OPL}(x, y)$ and the two $V_{Bip}(x, y)$) are normalized between -1 and 1, and passed through an adimensional rectification N as in Eq. (15) (with $i^0 = 0.3$, $\lambda = 1$, $v^0 = 0$, see Fig. 3(b)) modeling ganglion rectification and spike generation.

Panel B presents the rectified version of $I_{OPL}(x, y)$, the linear response. In panels C and D, we present the interplay between the rectified nonlinear output $V_{Bip}(x, y)$ and the adapting conductance $g_A(x, y)$ that produced the nonlinear effect.

In the case of a purely temporal contrast gain control ($\sigma_A = 0$, panel C), one can observe a re-equilibrating of the contrast levels, as compared to the linear output (B). Intermediate contrast levels are enhanced as compared to high-contrast levels (see, e.g., the small flower at the bottom left). Mathematically, when equilibrium is reached in Eqs. (11)–(13), one has the point-by-point relations $g_A(x, y) = Q(V_{Bip}(x, y)) = g_A^0 + \lambda_A V_{Bip}(x, y)^2$ and $I_{OPL}(x, y) = V_{Bip}(x, y) g_A(x, y)$, so that the nonlinear output can simply be understood as the static point-by-point compression

$$V_{Bip}(x, y) = L^{-1}(I_{OPL}(x, y)),$$

with $L(V) = V(g_A^0 + \lambda_A V^2)$. So in this case ($\sigma_A = 0$, on a static image), our gain control loop Eqs. (11)–(13) is close to a Gamma-transform (Gonzalez and Woods 1992) on the original linear output.

In the case where contrast gain control mechanism includes a spatial extent σ_A (panel D), the equilibrium between $V_{Bip}(x, y)$ and $g_A(x, y)$ becomes dependent on the spatial structure of the input image and there is no analytical expression. Intuitively, $g_A(x, y)$ provides a divisive effect on $V_{Bip}(x, y)$ based on the contrast *in the neighborhood* of (x, y), making $V_{Bip}(x, y)$ a measure of contrast that is *local* rather than absolute. This enhancement, which can be observed in the background in D, is very close to a local histogram equalization (see Gonzalez and Woods (1992), chapter 3) on the linear contrast image.

These results are another example of link between physiological and perceptual features allowed by large-scale simulation. We wish to stress the *qualitative* nature of these perceptual results on contrast gain control. For example, one might argue that we humans do not see such an enhanced contrast as that displayed in Fig. 11(d). It should not be forgotten that the Midget ('parvo') pathway of primates, which is supposed to be our primary source of precise form analysis, is very little subject to contrast gain control (Bernadete et al. 1992). Besides, the problem of 'double filtering' (by the software, and by our visual system) raises other issues concerning what we see when looking at the reconstructions.

To conclude, note that physiological measurements such as those of Shapley and Victor 78 (Fig. 6(a)) demonstrate that there is under-linearity to contrast in cat ganglion cells, at least in specific spatio-temporal conditions (their experiments concerned sinusoidal stimulation, whereas here we simulate a totally static image). This necessarily implies a perceptual invariance, for all cells which display contrast gain control (cat cells, primate Parasol ('magno') cells): At least, a static compression effect as in Fig. 11(c). Possibly, a local equalization as in Fig. 11(d).

4 Discussion

4.1 Customizable simulation software

4.1.1 Combining large-scale and plausibility

The first aim of this article was to present *Virtual Retina*, a large-scale simulation software. Before going into the details of the underlying retina model, we would like to stress the goals of this software: To achieve at the same time large-scale simulation and a relative biological plausibility, with an adaptable degree of complexity.

First of all, *Virtual Retina* is a *large-scale* simulator. It aims at providing input to neuroscientists who need this large-scale factor: Motion detection tasks in a natural scene, population coding by an assembly of spiking visual neurons, information-theoretic calculations on natural scenes. In this optic, it is being used by several research teams of the FACETS[5] European consortium as input to detailed models of primary visual cortex (V1). It can also serve as a demonstration tool in an educational framework.

As a large-scale simulator, we wished to reduce as much as possible the number of parameters used in the underlying model. This explains the simple form taken by our successive stages (OPL, contrast gain control, IPL and ganglion cells), that discard many effects known to occur in real retinas.

At the same time, *Virtual Retina* intends to be a *plausible* simulator, that can provide output spike trains reasonably close to those of real ganglion cells. The reproduction of a number of experimental recordings in Section 3 appeared a necessary step to prove the plausibility of the software.

As a plausible simulator, we wanted to keep specific properties of retinal processing that are often ignored by large-scale models. This includes: The non-separability of the OPL filter Eq. (10) that allows to detect both image edges and uniform flickering screens, the contrast gain control mechanism Eqs. (11)–(13) that provides invariance to contrast in natural scenes, and the trial-to-trial variability in the emission of spike trains.

As a plausible simulator also, *Virtual Retina* uses an underlying model mostly based on prior, state-of-the-art knowledge on the retina, experimental results as well as models. Our goal was to reduce this state-of-the-art knowledge to formulations as simple as possible, for inclusion in the software. As an exception, our contrast gain control mechanism based on conductances is a more original contribution, although it also strongly relates to previous work. The mechanism is discussed in the next paragraph. Note that potential users looking for purely state-of-the-art simulation can easily disconnect the contrast gain control stage, thanks to the modular nature of the software.

4.1.2 Subclasses of ganglion cells

In this section we shortly mention the different types of ganglion cells reproducible by our simulator. Names and classification of ganglion cells vary according to the species considered, and to the classification medium (morphology or physiology) (Kolb et al. 2001; Masland 2001). The goal of this section is not to review all types,

but just to give landmarks about retinal physiology and how our simulator relates to them.

In the cat retina, X and Y cells are the most studied type. Both types of cells display a strong contrast gain control (Shapley and Victor 1978), although the effect is stronger in Y cells. Y cells are more phasic, X cells more tonic. Finally, the response of Y cells cannot be modeled by linear spatial summation. Our model can account for both X and Y types of cellular response (see Section 3.2.1).

In the primate retina, *Midget* and *Parasol* cells have received the most attention. Midget cells are very precise spatially (small receptive field) and code for red-green color oppositions. They are known to display little contrast gain control (Kaplan and Bernadete 2001). They are connected to the Parvocellular pathway of the LGN, which is supposed to be in charge of precise shape detection. Parasol cells have a wider receptive field, are not sensitive to color but very sensitive to contrast, and display a strong contrast gain control effect. They are connected to the Magnocellular pathway of the LGN, which is supposed to be in charge of movement detection and broad scene analysis. Elements suggest that Midget cells constitute a new channel of visual information possessed only by primates, whereas Parasol cells are a common feature shared with other mammals, being close for example to cat X and Y cells (Kaplan and Bernadete 2001; Masland 2001). Following this hypothesis, *Virtual Retina* can reproduce primate Parasol cells with efficiency. Midget cells can also be reproduced in their achromatic features; but color oppositions are not handled yet by our model. Finally, as explained already, *Virtual Retina* handles the foveated structure typical of primate retinas.

Table 2 summarizes plausible orders of magnitude for the model parameters that must vary between cat and primate retinas. Values for σ_C and σ_S are taken from the literature (Enroth-Cugell and Robson (1966)

Table 2 Model parameters that vary according to species (cat and primate) and pathway

	Parameter	Cat X	Cat Y	Parasol	Midget
(*)	σ_C (deg)	0.15–0.8	0.15–0.8	0.03–0.1 (fov)	0.03–0.1 (fov)
(*)	σ_S (deg)	0.8–6	0.8–6	0.2–0.7 (fov)	0.2–0.7 (fov)
(?)	σ_A (deg)	0–1.5	0–1.5	0–0.2 (fov)	0–0.2 (fov)
(+)	σ_G (deg)	0	1.5	0–0.15 (fov)	0 (fov)
(+)	λ_A (Hz)	50–100	50–100	50–100	0
(+)	g_A^0 (Hz)	5	5	5	50
(+)	w_G	0.7	1	0.7–1	0.7
(+)	λ_G (Hz)	100	300	100–300	100

Plausible values for other parameters are in caption to Fig. 5. (*) Values taken from Enroth-Cugell and Robson (1966) (cat) and Croner and Kaplan (1995), McMahon et al. (2000) (primate). (+) Values which provided good fit to the model. Most of these parameters have equivalents in other retina models, with comparable values. (?) The adaptation spatial scale σ_A is a free parameter of the model, for which no data is available, only plausible orders of magnitude

for cat, Croner and Kaplan ([1995](#)), McMahon et al. ([2000](#)) for primate). Other parameters for cat cells are plausible orders of magnitude that provided good fit to data. Other parameters for primate cells are suggestions respecting the scaling from cat to primate retina, and the characteristics of primate cells explained in the above paragraph: Parasol cells can behave like cat X or Y cells, and Midget cells display no contrast gain control.

Remark Many other types of ganglion cells have been found in the cat retina (*W* cells, *Q* cells...) and in the primate retina (such as small bi-stratified ganglion cells which code for Blue/Yellow color opponents) with functionalities more or less known (Masland [2001](#); Wohrer [2008b](#)). Some are sensitive to illumination, others are tuned to directional movement (e.g., ON-OFF DS cells in rabbit retina), etc. Our model does not intend to reproduce these other subtypes, although we believe that for some of them, modeling is relatively straightforward from what is presented in this article.

4.1.3 Temporal transients and adaptation in the model

'Adaptation' is a word widely used in neurophysiology, that can convey various meanings. When presenting our model, we restricted this word to the description of nonlinear effects in retinal filtering. Conversely, we rather used the word 'transient' to define the temporal high-pass stages that we modeled through linear filters. Using this terminology, our simulator uses two linear transient filters T_{w_U,τ_U} and T_{w_G,τ_G}, and one contrast adaptation stage with the feedback loop Eqs. ([11](#))–([13](#)). We designed the feedback loop Eqs. ([11](#))–([13](#)) as a purely low-pass stage, by associating the adapting conductance g_A to a null Nernst potential. As a result, only the two linear filters T_{w_U,τ_U} and T_{w_G,τ_G} are in charge of temporal shaping in the system.

Our adaptation scheme to contrast is discussed in Section [4.2](#). We wish to stress that this scheme only aims to reproduce *fast* gain control adaptation. Recent works (Baccus and Meister [2002](#); Kim and Rieke [2001](#)) have revealed a second mechanism of gain control, on a much slower time scale. This secondary gain control enters the family of *slow adaptation* mechanisms in neurons, that we have not discussed nor included in our simulator. Likely, this slow adaptation is present simultaneously at different biological locations, both pre- and post-synaptically to ganglion cells.

In the salamander, Kim and Rieke ([2003](#), [2001](#)) find that slow contrast gain control could be accounted

for by a slow inactivation of Na$^+$ currents due to spike generation in the ganglion cells. In mammalian retinas, some studies (Solomon et al. ([2004](#)) in primate) also suggest that a large part of slow contrast adaptation arises directly in ganglion cells, while others (Manookin and Demb ([2006](#)) in guinea pig) suggest that slow adaptation is mostly presynaptic to the ganglion cells, because currents directly injected in ganglion cells induce less slow adaptation.

For the moment, *Virtual Retina* ignores slow adaptation, although a very experimental spike-frequency adaptation scheme is available in the source code. Note that if a slow adaptation was implemented in the model (spike-frequency adaptation or other), it would allow to account for the nonlinear variations of cat X cells in response to a uniform screen, according to their mean level of activity during the current stimulation (Section [3.2.1](#) and Fig. [4](#)(a)).

As for linear filters T_{w_U,τ_U} in Eq. ([8](#)) and T_{w_G,τ_G} in Eq. ([14](#)), they must be seen as a functionally convenient choice to reproduce band-pass behaviors in the retina. Their respective biological locations and time scales (100 ms for T_{w_U,τ_U} versus $10-30$ ms for T_{w_G,τ_G}) do not intend to reproduce physiology with precision.

T_{w_U,τ_U} in Eq. ([8](#)) can be associated to different physiological meanings: First, it is a crude approximation of the intrinsic undershoot occurring in cone photo-transduction in the time scales of a few hundreds of milliseconds (Schnapf et al. [1990](#)). At the same time, it provides a very simple linear equivalent to slow cellular adaptation described in the previous paragraph. Finally, it serves as a way to correctly enhance the $1-10$ Hz frequency range before application of the contrast gain control stage (see Section [3.2.2](#) and Fig. [6](#)(d)).

By opposition, T_{w_G,τ_G} in Eq. ([14](#)) is rather associated to fast transients which occur later in retinal processing due to retinal connectivity. It accounts mostly for amacrine cells that provide a strong inhibition on some bipolar cells and/or ganglion cells at the level of synapses in the IPL. T_{w_G,τ_G} is the processing step where we can fix the balance between tonic and phasic cells, through parameter w_G (Section [2.4.1](#)). Biologically, locating the tonic/phasic opposition at the level of the IPL is reasonable, since the IPL is the retinal location with the biggest variety of cell subtypes (Masland [2001](#)), by opposition with the OPL that involves only two types of light receptors (cones and rods) and three to four types of horizontal cells (Kolb et al. [2001](#); Masland [2001](#)). Bipolar cells are known to exist under different subtypes with different band-pass properties (Masland [2001](#)), possibly reflecting different interactions at their synaptic terminals in the IPL.

4.2 Contrast gain control mechanism

A key feature of the present model is its detailed contrast gain control stage Eqs. (11)–(13), and how it relates to experimental observations (Section 3.2.2). Here we discuss the biological relevance of our model, and relate it to other gain-control models that have been proposed at the level of the retina.

Shunt conductances   Our model assumes that fast contrast gain control is achieved by the divisive influence of conductances in the membrane of bipolar cells. When a conductance $g_j(t)$ opens in a cellular membrane, associated to *Nernst* potential E_j, it creates a synaptic current $g_j(t)(E_j - V(t))$ through the membrane, as detailed in equation (1). Such a current can be decomposed in a 'linear contribution' $g_j(t)E_j$ and a 'shunt contribution' $-g_j(t)V(t)$. If only the first term is taken into account, then $g_j(t)$ contributes linearly to $V(t)$. The second term, by opposition, is independent of the Nernst potential, and modifies nonlinearly the instantaneous gain of membrane integration.

At the contrast gain control stage Eqs. (11)–(13), our model focuses on the *shunting* impact of dynamic conductances onto bipolar cells: Only the term $-g_A(t)V(t)$ is present, as if our adapting conductance g_A was associated to a null Nernst potential. We do not claim this to be the biological reality, but only a computational convenience to reduce the number of required parameters. First, it dispenses from fixing a value to the Nernst potential. More importantly, it allows the whole scheme Eqs. (11)–(13) to display an ON-OFF symmetry, which provides a fair reduction in the number of parameters.

ON-OFF symmetry   In the retina, the positive and negative parts of visual signals are transmitted through two distinct pathways, ON and OFF, that imply different cells. Our model takes this distinction into account starting at Eq. (14), right before spike generation by ganglion cells. Before that, single signals (I_{OPL}, V_{Bip}...) are used, which code symmetrically for positive and negative values. In real retinas, the distinction arises earlier, through ON and OFF bipolar cells. The former are somewhat slower (mostly, because of a metabotropic receptor required to invert the polarity of the photoreceptor signal), less subject to contrast gain control, and more numerous than OFF cells (Chichilnisky and Kalmar 2002; Rieke 2001; Kolb et al. 2001).

Our contrast gain control scheme Eqs. (11)–(13), which is totally symmetrical, is thus a consequent simplification of the biological reality, in order to reduce model complexity. This explains the symmetric shape

of function Q, not often met in biological neurons: it is intended to encompass simultaneously gain controls on ON and OFF cells. The corresponding biological architecture, if it exists, is that of two distinct pathways which display:

- A gain control mechanism on their preferred contrast polarity (ON or OFF), similarly to Eqs. (11)–(13), except for function Q that becomes a one-sided smooth rectification (similar to function N in Eq. (15)).
- A signal compression on their non-preferred contrast polarity.

Convex activation function   The quadratic expression chosen here for Q is the simplest function to be both symmetrical and flat around $V_{Bip} = 0$. This flatness around zero was found mandatory to reproduce the multi-sinus kernels of Section 3.2.2. For example, similar good reproduction was obtained when function Q was linear by parts with an activation threshold:

$$Q(V_{Bip}) = \begin{cases} g_A^0 & \text{if } 0 < V_{Bip} < v_0, \\ g_A^0 + \lambda_A(V_{Bip} - v_0) & \text{if } V_{Bip} > v_0, \end{cases}$$

and symmetrically in the negative range. But this required a supplementary parameter, and allowed a less well-defined mathematical analysis.

Biologically, the convex shape required for Q in our model might reflect the existence of voltage-gated conductances in bipolar cells, whose activation becomes significant only at high potentials V_{Bip}. Indeed, different voltage-gated inhibitory currents have been observed in bipolar cells of several species (Connaughton and Maguire 1998; Kolb et al. 2001). Mathematically, the convexity of Q is also an important property, as demonstrated in Wohrer (2007): We refer to Appendix B for the main result.

Physiological interpretation   It is natural to ask whether or not the present model of gain control can be attached to a physiological meaning. Experiment has established that the *fast* gain control mechanism (Baccus and Meister 2002) is already observed at the level of bipolar cells (Rieke 2001).

But what could be the biological origin of conductances g_A in the membranes of bipolar cells, as in our model? From the discovery of the contrast gain control effect and on (Shapley and Victor 1978), it was believed the effect had a link with amacrine cells, and/or the so-called 'sub-units' of Hochstein and Shapley (1976). However, recent experimentations have revealed that the fast contrast gain control effect is still present under physiological blockade of amacrine synapses (Rieke 2001; Beaudoin et al. 2007). These findings likely

eliminate the hypothesis that g_A arises from amacrine synapses.

One plausible explanation is that g_A arises from *voltage-gated conductances* in the membranes of bipolar cells. Voltage-gated conductances have already been hypothesized to contribute to contrast gain control in mammalian bipolar cells (Mao et al. 1998). This would explain the direct dependence of g_A on the recent values of $V_{Bip}(x, y, t)$, as well as the small time scale τ_A for the adaptation, that we found to produce the best results in our simulations (τ_A=5 ms).

Another possible explanation could imply *calcium adaptation*, often hypothesized as a source of contrast gain control in bipolar cells (Shiells and Falk 1999; Nawy 2000; Rieke 2001). Modeling calcium feedbacks often leads to systems formally close to Eqs. (11)–(13) (see, e.g., the phototransduction model of van Hateren and Lamb (2006)), but with a different physiological interpretation of the system variables. In this alternative interpretation, the 'controlled' variable (V_{Bip} in Eqs. (11)–(13)) is the input dendritic current I_{Syn} on bipolar cells, while the 'controlling' variable (g_A in Eqs. (11)–(13)) is the concentration of some calcium-binding molecule $[M]$, which regulates I_{Syn} through a catalyzer equation formally similar to (11). Finally, a convex nonlinearity Q may also be introduced for different reasons: Possibly, a Hill exponent in the binding of calcium to molecule $[M]$.

In both biological interpretations (voltage-gated conductances or calcium adaptation), the contrast gain control mechanism could have a certain *spatial extent* σ_A, due to a diffusion of the molecules or ions involved in the control reaction (e.g., a diffusion of Ca^{2+}, in the 'calcium' interpretation of the model). Such diffusion is indeed possible, due to the existence of gap junctions between neighboring bipolar cells (Dacey et al. 2000; Kolb et al. 2001). We have seen in Section 3.3.2 how the presence or not of the diffusion through parameter σ_A has perceptual consequences on the output of our gain control model.

Other models of gain control How does our model compare with other gain control models in the retina? The main influence of our gain control model is that of Victor (1987). His empirical model reproduces changes in the Wiener kernel due to contrast, thanks to a high-pass filtering stage whose time constant is a function of the recent values of contrast. His model is also based on a dynamical feedback mechanism.

The main difference in our model is that we associate contrast gain control Eqs. (11)–(13) to a *low-pass* scheme only. Temporal high-pass is done through purely linear filters, before (slow transient T_{w_U, τ_U} in

Eq. (8)) and after (fast transient T_{w_G, τ_G} in Eq. (14)) our gain control loop. Our gains by doing so are:

- Conceptual separation of two distinct effects, since a low-pass model is simpler, and sufficient to account for the contrast gain control.
- More biological plausibility, since our mechanism can be associated to a biological signification.
- A mathematically tractable model, with available proofs concerning the behavior of the control loop (see Appendix B).

We also extended Victor's concept of 'local level of contrast' to a possible spatial extent σ_A (the Victor 87 model is purely temporal), and observed its possible consequences on a perceptual level.

However, our gain control model remains the direct descent of the Victor model, one of the most accurate models of contrast gain control in the retina, that served as a direct influence to more recent models, such as the Y cell model of Enroth-Cugell and Freeman (1987), or the Van Hateren model for primate Parasol cells (van Hateren et al. 2002).

Another source of inspiration for our model can be found in models that propose *spatial* divisive effects in the retina. This is the case of the Bonin LGN model (Bonin et al. 2005) which proposes the idea of a divisive *spatial* surround. Similarly, the Herault et al. retina model (Hérault and Durette 2007) allows at the same time for luminance and contrast invariance, through two successive divisive steps in retinal processing. Their model, strongly oriented towards fast image processing, displays purely analogical signals (no spikes), and does not focus on the temporal shaping of ganglion responses by temporal transients like our model. Neither Bonin nor Herault models are concerned with the dynamical change in the Wiener kernel induced by contrast gain control, but only by the *spatial* divisive influence of luminance and/or contrast on retinal outputs.

To summarize, two 'trends' of gain control models can be found: Those based on the temporal expression of the gain control and those based on its spatial expression. Here we proposed a framework where both effects can be accounted for, while bearing possible biological interpretations.

5 Conclusion

In this article we described the underlying model and main characteristics of the open-source simulation software *Virtual Retina*. Interestingly, this software can emulate up to around 100,000 cells with a processing speed of about 1/100 real time, which makes it a good

choice for large-scale simulations of the visual cortex (and possibly LGN) that require a realistic input from the retina. The first stage of the model corresponds to the OPL modeled as a non-separable spatio-temporal linear filter. The second stage is an original implementation of contrast gain control through a shunting feedback mechanism. The third stage concerns further temporal shaping in the IPL and spike generation in ganglion cells, to form the output spike trains.

Of course, this simulator remains an abstraction of the precise retinal mechanisms. It relies on assumptions and simplifications necessary to have an efficient simulator. However, in all this work, strong efforts were made to justify the modeling choices thanks to physiology literature.

Introducing nonlinearities was one focus of the simulator. For example, we proposed an original contrast gain control mechanism based on a system of ordinary differential equations, which can implement both spatial and temporal invariance to contrast, and for which mathematical results have been established. Another kind of nonlinearity modeled in the software is the spatial nonlinearity of cat Y cells.

Another goal was to build a modular software, with an adaptable degree of complexity for the underlying retinal model. The retina models used by *Virtual Retina* have a structure and internal parameters which are all defined in a single customizable XML file, with adaptable complexity.

In its present state, we see three main types of applications for the simulator in the field of visual neuroscience. The first type of application is to use the software as a bio-plausible input to models of higher-level visual processing – typically, LGN or V1. As such, the simulator could advantageously replace the over-simplified retina models generally used as input. Such usage of the software has started amongst laboratories of the FACETS EC IP project.

A second type of application is to use the software as a tool to understand retinal coding itself. In this scope, we are currently developing advanced reconstruction procedures from the spiking output of a retina, exploiting the particular filtering structure with a delayed *surround* signal.

More generally, we have shown in this article first qualitative examples of how the constitutive elements of the retina model (nature of the linear filter, contrast gain control) have a strong influence on large-scale percepts. We are now seeking methods to *quantitatively* assess the perceptual quality of retinal transmission: Suppose we can compute, for a given retina, a finite number of statistical estimators $\{X_\alpha\}$ measuring how efficiently this retina transmits a set $\{\alpha\}$ of 'perceptual

descriptors' for natural scenes.[6] Then, *Virtual Retina* can be used to measure the evolution of the various estimators $\{X_\alpha\}$ according to the parameters of the retina model. The *perceptual* influences of the non-separable center-surround filtering (Section 2.2, and Fig. 10), of contrast gain control (Section 2.3, and Fig. 11), or of the non-Poisson spiking statistics induced by the nLIF model (Section 2.4.2), could thus be quantified in terms of their impact on the various estimators $\{X_\alpha\}$.

Finally, a third application is to use the software for educational purposes, e.g., through its webservice interface, to efficiently illustrate the nature of retinal coding.

To conclude, we would like to mention that *Virtual Retina* is an evolutionary software: Depending on user's requirements, other features could be integrated, such as realistic eye movements (pure rotation), chromatic oppositions, stimulus-dependent synchrony between the spikes of neighboring cells, or fitting of parameters to build a feed-forward model of LGN.

Appendix A - Coupling kernel in a layer of cells

Let us comment further the choice of the convolution kernel $G_\sigma E_\tau(x, y, t)$ to model signal averaging in a layer of cells (see Section 2.1.3). Suppose that a layer of retinal cells, described by the spatially continuous potential $V(x, y, t)$, is linearly driven by an input synaptic current $I(x, y, t)$. Then, V can always be linearly calculated from I, through an *impulse response* $K(x, y, t)$:

$$V(x, y, t) = K * I(x, y, t), \tag{19}$$

where symbol $*$ represents spatio-temporal convolution. Because neurons are small 'RC' circuits, K is temporally low-pass, with a term in $\exp(-t/\tau)$. However, the precise expression of K depends on the type of spatial averaging being modeled. There are two effects:

- Averaging because of the cells' *dendritic spread* is well modeled by a static spatial Gaussian kernel,

---

leading to the separable filter

$$K_{\text{dendritic spread}}(x, y, t) = G_\sigma(x, y) \exp(-t/\tau). \quad (20)$$

- Averaging by *gap junctions* between neighboring cells can be expressed either in a discrete-cell approach (Mahowald and Mead 1991; Herault 1996) or in a continuous setting with Laplacian-like operators (Naka and Rushton 1967; Lamb 1976). Both approaches lead approximately to the same impulse response

$$K_{\text{gap junctions}}(x, y, t) = G_{\sqrt{2\mathcal{G}t}}(x, y) \exp(-t/\tau), \quad (21)$$

where $\mathcal{G}$ is a constant measuring the two-dimensional density of gap junctions.

One can verify that both Eqs. (20) and (21) are spatio-temporal low-pass filters, with very similar characteristics in the Fourier domain. Filter Eq. (21) is a bit harder to handle mathematically, because of the influence of time t on the spatial Gaussian kernel. For this reason, in this article we model all low-pass effects, including effect of gap junctions, with separable filters like Eq. (20). However, the filtering kernel Eq. (21) is also implemented in *Virtual Retina*.

Appendix B - Mathematical analysis of the contrast gain control loop

An original contribution in this work was the proposition of a contrast gain control mechanism (Section 2.3) *via* the differential equation

$$\frac{dV}{dt}(x, y, t) = I_{\text{OPL}}(x, y, t) - g_A(x, y, t)V(x, y, t) \quad (22)$$

with

$$g_A(x, y, t) = G_{\sigma_A} \overset{x,y}{*} E_{\tau_A} \overset{t}{*} Q(V) \ (x, y, t), \quad (23)$$

$$Q(V) = g_A^0 + \lambda_A V^2. \quad (24)$$

Mathematically, this dynamical system is difficult to study due to its high dimensionality (two variables V and g_A, expressed on spatial maps). Thus, in Wohrer (2007), we studied the simplified dynamical system

$$\frac{dV}{dt}(t) = A \cos(\omega t) - V(t)Q(V(t)), \quad (25)$$

for which we can prove contrast gain control properties. System (25) derives from (22) considering the following assumptions:

- We considered a sinusoidal stimulation: $I_{\text{OPL}}(t) = A \cos(\omega t)$. This is the simplest way to control both

amplitude A (i.e., *contrast*) and speed of temporal variation ω in the input. Furthermore, sinusoidal stimulation enables direct comparison of our system with linear ones, for which Fourier analysis can be done.

- We assumed that $\sigma_A = 0$, so that (25) depends only on time t, and not on any spatial structure (x, y). This choice does not appear too restrictive, especially since contrast gain control is experimentally settled as a *temporal* property only (see Section 4.2).

- We consider the asymptotic limit of Eq. (22), when parameter τ_A in (23) tends to zero, yielding $g_A(t) = Q(V_{\text{Bip}}(t))$. As a consequence, (25) is now a *one-dimensional dynamical system*, easier to study. The assumption $\tau_A \simeq 0$ is justified in the scope of our simulations, for which we chose a small constant $\tau_A = 5$ ms, as detailed in Sections 3.2.2 and 4.2.

In Wohrer (2007), we proved general properties of system (25).

First, (25) is a very stable system. Similarly to a simple linear exponential filter, the system (25) forgets its initial condition exponentially fast (Lohmiller and Slotine 1998): All trajectories converge asymptotically to a unique solution $V(t)$ which is $\frac{2\pi}{\omega}$-periodic (like the input current).

Furthermore, over one cycle, $V(t)$ reaches a single maximum V_{max} at time t_{max}, and a single minimum $V_{\text{min}} = -V_{\text{max}}$ at time $t_{\text{min}} = t_{\text{max}} - \pi/\omega$. In Wohrer (2007), we studied V_{max} as a measure of the *strength* of the system's response to the input current, and ωt_{max} as a measure of the *phase* of the system's response to the input current.

By studying V_{max} and t_{max}, we thus provided a description of the system's behavior according to input frequency and amplitude. This is presented in the following theorem, which shows that (25) acts as a *low-pass*, *gain control* system on its input, given suitable assumptions on Q.

Theorem 1 *Let V be a solution of* (25), *with Q an even, convex and strictly positive function. First, we show how V_{max} and ωt_{max} depend on the frequency ω:*

(i) *Low-pass setting*

$$\partial_\omega V_{\text{max}} < 0 \ \ and \ \ \lim_{\omega \to +\infty} V_{\text{max}} = 0.$$

(ii) *Phase delay*

$$\partial_\omega(\omega t_{\text{max}}) > 0 \ \ and \ \ \lim_{\omega \to +\infty} \omega t_{\text{max}} = \frac{\pi}{2} \ (mod \ 2\pi).$$

Second, we show how V_{max} and ωt_{max} depend on the amplitude A:

```
<retina-description-file>

    <retina temporal-step__sec="0.005"
            input-luminosity-range="255"
            pixels-per-degree="2.0">

        <outer-plexiform-layer>
          <undershoot-version
             center-sigma__deg="0.88"
             surround-sigma__deg="2.35"
             center-tau__sec="0.01"
             center-n__uint="2"
             surround-tau__sec="0.01"
             opl-amplification="10"
             opl-relative-weight="1"
             leaky-heat-equation="0"
             undershoot-relative-weight="0.8"
             undershoot-tau__sec="0.1"/>
        </outer-plexiform-layer>

        <contrast-gain-control
             opl-amplification__Hz="100"
             bipolar-inert-leaks__Hz="5"
             adaptation-sigma__deg="2.5"
             adaptation-tau__sec="0.005"
             adaptation-feedback-amplification__Hz="50"/>

        <ganglion-layer
             sign = "-1"
             transient-tau__sec="0.02"
             transient-relative-weight="0.7"
             bipolar-linear-threshold="0"
             value-at-linear-threshold__Hz="80"
             bipolar-amplification__Hz="150"
             sigma-pool__deg="0">
                <spiking-channel>
                  <circular-spiking-channel
                     diameter__deg="1" fovea-density__inv-deg="1"
                     g-leak__Hz="50" sigma-V="0.1" refr-mean__sec="0.003"
                     refr-stdev__sec="0.001" random-init="1" />
                </spiking-channel>
        </ganglion-layer>

    </retina>
</retina-description-file>
```

Fig. 12 Sample XML file used by *Virtual Retina* to load the architecture and parameters of the used model. This file is highly modular

(iii) *Growth of $V_{\max}$*

$$\partial_A V_{\max} > 0 \quad and \quad \lim_{A \to +\infty} V_{\max} = +\infty.$$

(iv) *Phase advance*

$$\partial_A t_{\max} < 0 \quad and \quad \lim_{A \to +\infty} \omega t_{\max} = 0 \ (mod \ 2\pi).$$

(v) *Under-linearity*

$$\forall (\omega, Q), \ \ if \ A \ is \ high \ enough, \ \ \partial_A \frac{V_{\max}}{A} < 0.$$

$$Also, \quad \lim_{A \to +\infty} \frac{V_{\max}}{A} = 0.$$

Let us comment those results.

Properties (i) and (ii) show that system (25) acts as a *low-pass* temporal filter (using a classical linear systems terminology). To understand this, suppose that $Q(V) = g_A^0$, i.e., just a constant function. This means having a null feedback strength λ_A in Eq. (24). Then, Eq. (25) becomes a simple exponential low-pass filter

$$\dot{V}(t) = A \cos(\omega t) - g_A^0 V(t), \tag{26}$$

whose behavior is well known:

$$V_{\max} = |\widetilde{H}(\omega)| A \tag{27}$$

$$\omega t_{\max} = \arg(\widetilde{H}(\omega)), \tag{28}$$

where $\widetilde{H}(\omega) = 1/(g_A^0 + \mathbf{j}\omega)$ is the Fourier transform of the system. One verifies easily that Eqs. (27)–(28) imply that $V_{\max}$ tends to 0 (with $V_{\max} > 0$) and $\omega t_{\max}$ tends to $\frac{\pi}{2}$ ($\omega t_{\max} < \frac{\pi}{2}$), as $\omega \to +\infty$. Properties (i)–(ii) extend these properties in the nonlinear case of (25).

Properties (iii), (iv) and (v) show the apparition of *gain control* in system (25), as opposed to the linear case (26). In the linear case, Eqs. (27)–(28) give a *linear* dependence of $V_{\max}$ and $t_{\max}$ with respect to amplitude A. One has indeed $\partial_A V_{\max} = |\widetilde{H}(\omega)| > 0$, $\partial_A(V_{\max}/A) = 0$ and $\partial_A(\omega t_{\max}) = 0$. In the nonlinear case (25), property (iii) shows that $V_{\max}$ is still a growing function of A. However, this growth is now *under-linear* (property (v)).

Finally, property (iv) shows the *phase advance* effect, with input amplitude A. This second nonlinear effect corresponds to the definition of contrast gain control in real retinas, as detailed in Section 3.2.2.

Appendix C - Example of an XML configuration file

Figure 12 is a snapshot from an XML definition file used in the simulator (with basis parameters for the X

cell modeled in Fig. 5(a)). Various XML nodes – such as contrast gain control or the spiking array – can be present or absent from the file, adapting the simulated model's complexity in consequence.

In particular, a radial scheme can be present or not (here it is useless because a single cell is modeled). The spiking array can either be square, or made of concentric circles following retinal density (as here). In this example file, given the parameters of the circular spiking array, a single spiking cell is present (as used for reproduction of physiological recordings).

References

Baccus, S., & Meister, M. (2002). Fast and slow contrast adaptation in retinal circuitry. *Neuron, 36*(5), 909–919.

Bálya, D., Roska, B., Roska, T., & Werblin, F. S. (2002). A CNN framework for modeling parallel processing in a mammalian retina. *International Journal of Circuit Theory and Applications, 30*(2–3), 363–393.

Barlow, H. B. (1953). Action potentials from the frog's retina. *Journal of Physiology, 119*(1), 58–68.

Beaudoin, D. L., Borghuis, B. G., & Demb, J. B. (2007). Cellular basis for contrast gain control over the receptive field center of mammalian retinal ganglion cells. *Journal of Neuroscience, 27*, 2636–2645.

Bernadete, E. A., & Kaplan, E. (1999). Dynamics of primate P retinal ganglion cells: Responses to chromatic and achromatic stimuli. *Journal of Physiology, 519*(3), 775–790.

Bernadete, E. A., Kaplan, E., & Knight, B. W. (1992). Contrast gain control in the primate retina: P cells are not X-like, some M cells are. *Visual Neuroscience, 8*(5), 483–486.

Berry, M. J., Warland, D. K., & Meister, M. (1997). The structure and precision of retinal spike trains. *Proceedings of the National Academy of Sciences of the United States of America, 94*, 5411–5416.

Bonin, V., Mante, V., & Carandini, M. (2005). The suppressive field of neurons in lateral geniculate nucleus. *Journal of Neuroscience, 25*(47), 10844–10856, November.

Cai, D., Deangelis, G. C., & Freeman, D. (1997). Spatiotemporal receptive field organization in the lateral geniculate nucleus of cats and kittens. *Journal of Neurophysiology, 78*(2), 1045–1061, August.

Carandini, M., Demb, J. B., Mante, V., Tollhurst, D. J., Dan, Y., Olshausen, B. A., et al. (2005). Do we know what the early visual system does? *Journal of Neuroscience, 25*(46), 10577–10597, November.

Chichilnisky, E. J. (2001). A simple white noise analysis of neuronal light responses. *Network: Computation in Neural Systems, 12*, 199–213.

Chichilnisky, E. J., & Kalmar, R. S. (2002). Functional asymmetries in ON and OFF ganglion cells of primate retina. *Journal of Neuroscience, 22*(7), 2737–2747, April.

Connaughton, V. P., & Maguire, G. (1998). Differential expression of voltage-gated K+ and Ca2+ currents in bipolar cells in the zebrafish retinal slice. *European Journal of Neuroscience, 10*(4), 1350–1362, April.

Croner, L. J., & Kaplan, E. (1995). Receptive fields of P and M ganglion cells across the primate retina. *Vision Research, 35*(1), 7–24, January.

Dacey, D., Packer, O. S., Diller, L., Brainard, D., Peterson, B., & Lee, B. (2000). Center surround receptive field structure of cone bipolar cells in primate retina. *Vision Research, 40*, 1801–1811.

Dacey, D., & Petersen, M. (1992). Dendritic field size and morphology of midget and parasol ganglion cells of the human retina. *Proceedings of the National Academy of Sciences, 89*, 9666–9670.

Delorme, A., Gautrais, J., VanRullen, R., & Thorpe, S. J. (1999). Spikenet: A simulator for modeling large networks of integrate and fire neurons. *Neurocomputing, 26*, 989–996.

Demb, J. B., Zaghloul, K., Haarsma, L., & Sterling, P. (2001). Bipolar cells contribute to nonlinear spatial summation in the brisk-transient (Y) ganglion cell in mammalian retina. *Journal of Neuroscience, 21*(19), 7447–7454, October.

Dhingra, N. K., & Smith, R. G. (2004). Spike generator limits efficiency of information transfer in a retinal ganglion cell. *Journal of Neuroscience, 24*, 2914–2922.

Enroth-Cugell, C., & Freeman, A. W. (1987). The receptive-field spatial structure of cat retinal Y cells. *Journal of Physiology, 384*(1), 49–79.

Enroth-Cugell, C., & Robson, J. G. (1966). The contrast sensitivity of retinal ganglion cells of the cat. *Journal of Physiology, 187*, 517–552.

Enroth-Cugell, C., Robson, J. G., Schweitzer-Tong, D. E., & Watson, A. B. (1983). Spatio-temporal interactions in cat retinal ganglion cells showing linear spatial summation. *Journal of Physiology, 341*, 279–307.

Erwin, H. (2004). http://scat-he-g4.sunderland.ac.uk/harryerw/phpwiki/index.php/tonicphasic.

Euler, T., & Masland, R. H. (2000). Light-evoked responses of bipolar cells in a mammalian retina. *Journal of Neurophysiology, 83*(4), 1817–1829, April.

Flores-Herr, N., Protti, D. A., & Wässle, H. (2001). Synaptic currents generating the inhibitory surround of ganglion cells in the mammalian retina. *Journal of Neuroscience, 21*(13), 4852–4863, July.

Gazeres, N., Borg-Graham, L., & Fregnac, Y. (1998). A phenomenological model of visually evoked spike trains in cat geniculate nonlagged X-cells. *Visual Neuroscience, 15*, 1157–1174.

Gollisch, T., & Meister, M. (2008). Rapid neural coding in the retina with relative spike latencies. *Science, 319*, 1108–1111. doi:10.1126/science.1149639.

Gonzalez, R. C., & Woods, R. E. (1992). *Digital image processing*, 3rd edn. Redwood City: Addison Wesley.

Hartveit, E., & Heggelund, P. (1994). Response variability of single cells in the dorsal lateral geniculate nucleus of the cat. Comparison with retinal input and effect of brain stem stimulation. *Journal of Neurophysiology, 72*(3), 1278–1289.

Hennig, M. H., Funke, K., & Wörgötter, F. (2002). The influence of different retinal subcircuits on the nonlinearity of ganglion cell behavior. *Journal of Neuroscience, 22*(19), 8726–8738, October.

Herault, J. (1996). A model of colour processing in the retina of vertebrates: From photoreceptors to colour opposition and colour constancy phenomena. *Neurocomputing, 12*, 113–129.

Hérault, J., & Durette, B. (2007). Modeling visual perception for image processing. In F. Sandoval, A. Prieto, J. Cabestany, M. Gra na, (Eds.), *Computational and ambient intelligence : 9th international work-conference on artificial neural networks, IWANN 2007* (pp. 662–675). Springer.

Hochstein, S., & Shapley, R. M. (1976). Linear and nonlinear spatial subunits in Y cat retinal ganglion cells. *Journal of Physiology, 262*, 265–284.

Jacobs, A. L., & Werblin, F. S. (1998). Spatiotemporal patterns at the retinal output. *Journal of Neurophysiology, 80*(1), 447–451, July.

Kaplan, E., & Bernadete, E. (2001). The dynamics of primate retinal ganglion cells. *Progress in Brain Research, 134*, 1–18.

Kara, P., Reinagel, P., & Reid, R. C. (2000). Low response variability in simultaneously recorded retinal, thalamic, and cortical neurons. *Neuron, 27*(3), 635–646. Poisson, retina, spike variability.

Keat, J., Reinagel, P., Reid, R. C., & Meister, M. (2001). Predicting every spike: A model for the responses of visual neurons. *Neuron, 30*, 803–817.

Kenyon, G. T., & Marshak, D. W. (1998). Gap junctions with amacrine cells provide a feedback pathway for ganglion cells within the retina. *Proceedings of the Royal Society B, 265*(1399), 919–925, May.

Kenyon, G. T., Theiler, J., George, J. S., Travis, B. J., & Marshak, D. W. (2004). Correlated firing improves stimulus discrimination in a retinal model. *Neural Computation, 16*, 2261–2291.

Kim, K. J., & Rieke, F. (2001). Temporal contrast adaptation in the input and output signals of salamander retinal ganglion cells. *Journal of Neuroscience, 21*(1), 287–299, January.

Kim, K. J., & Rieke, F. (2003). Slow Na+ inactivation and variance adaptation in salamander retinal ganglion cells. *Journal of Neuroscience, 23*(4), 1506–1516, February.

Kolb, H., Fernandez, E., & Nelson, R. (2001). Webvision: The organization of the retina and visual system. http://webvision.med.utah.edu/.

Kuffler, S. W. (1953). Discharge patterns and functional organization of mammalian retina. *Journal of Neurophysiology, 16*, 37–68.

Lamb, T. D. (1976). Spatial properties of horizontal cell responses in the turtle retina. *Journal of Physiology, 263*(2), 239–55.

Lesica, N. A., & Stanley, G. B. (2004). Encoding of natural scene movies by tonic and burst spikes in the lateral geniculate nucleus. *Journal of Neuroscience, 24*(47), 10731–10740.

Lohmiller, W., & Slotine, J. J. (1998). On contraction analysis for non-linear systems. *Automatica, 34*(6), 683–696, June.

McMahon, M. J., Lankheet, M. J. M., Lennie, P., & Williams, D. R. (2000). Fine structure of parvocellular receptive fields in the primate fovea revealed by laser interferometry. *Journal of Neuroscience, 20*(5), 2043–2053, March.

McMahon, M. J., Packer, O. S., & Dacey, D. M. (2004). The classical receptive field surround of primate Parasol ganglion cells is mediated primarily by a non-GABAergic pathway. *Journal of Neuroscience, 24*(15), 3736–3745, April.

Mahowald, M. A., & Mead, C. (1991). The silicon retina. *Scientific American, 264*(5), 76–82.

Manookin, M., & Demb, J. (2006). Presynaptic mechanism for slow contrast adaptation in mammalian retinal ganglion cells. *Neuron, 50*(3), 453–464.

Mao, B. U. Q., Macleish, P. R., & Victor, J. D. (1998). The intrinsic dynamics of retinal bipolar cells isolated from tiger salamander. *Visual Neuroscience, 15*(3), 425–438.

Marmarelis, P. Z., & Naka, K. (1972). White-noise analysis of a neuron chain, an application of the Wiener theory. *Science, 175*(4027), 1276–1278, March.

Martinez-Conde, S., Macknik, S. L., & Hubel, D. H. (2004). The role of fixational eye movements in visual perception. *Nature Reviews Neuroscience, 5*, 229–240.

Masland, R. (2001). The fundamental plan of the retina. *Nature Neuroscience, 4*(9), 877–886, September.

Moisan, M. (2007). http://www.flickr.com/photos/marchelino/.

Naka, K. I., & Rushton, W. A. (1967). The generation and spread of s-potentials in fish (cyprinidae). *Journal of Physiology, 192*(2), 437–61, September.

Nawy, S. (2000). Regulation of the On bipolar cell mGluR6 pathway by Ca2+. *Journal of Neuroscience, 20*(12), 4471.

Neuenschwander, S., & Singer, W. (1996). Long-range synchronization of oscillatory light responses in the cat retina and lateral geniculate nucleus. *Nature, 379*(6567), 728–732, February.

Nirenberg, S., & Meister, M. (1997). The light response of retinal ganglion cells is truncated by a displaced amacrine circuit. *Neuron, 18*, 637–650.

O'Brien, B. J., Isayama, T., Richardson, R., & Berson, D. M. (2002). Intrinsic physiological properties of cat retinal ganglion cells. *Journal of Physiology, 538*(3), 787–802.

Polans, A., Baehr, W., & Palczewski, K. (1996). Turned on by Ca^{2+}! The physiology and pathology of Ca^{2+}-binding proteins in the retina. *Trends in Neurosciences, 19*(12), 547–554, December.

Raviola, E., & Gilula, N. B. (1973). Gap junctions between photoreceptor cells in the vertebrate retina. *Proceedings of the National Academy of Sciences, 70*(6), 1677–1681, June.

Rieke, F. (2001). Temporal contrast adaptation in salamander bipolar cells. *Journal of Neuroscience, 21*(23), 9445–9454, December.

Roska, B., & Werblin, F. (2001). Vertical interactions across ten parallel, stacked representations in the mammalian retina. *Nature, 410*, 583–7, March.

Van Rullen, R., & Thorpe, S. (2001). Rate coding versus temporal order coding: What the retina ganglion cells tell the visual cortex. *Neural Computing, 13*(6), 1255–1283.

Schnapf, J. L., Nunn, B. J., Meister, M., & Baylor, D. A. (1990). Visual transduction in cones of the monkey macaca fascicularis. *Journal of Physiology, 427*(1), 681–713.

Shapley, R. M., & Victor, J. D. (1978). The effect of contrast on the transfer properties of cat retinal ganglion cells. *Journal of Physiology, 285*(1), 275–298.

Shiells, R. A., & Falk, G. (1999). A rise in intracellular Ca2+ underlies light adaptation in dogfish retinal 'on' bipolar cells. *Journal of Physiology, 514*(2), 343–350.

Solomon, S. G., Peirce, J. W., Dhruv, N. T., & Lennie, P. (2004). Profound contrast adaptation early in the visual pathway. *Neuron, 42*, 155–162, April.

Tan, S., Dale, J., & Johnston, A. (2003). Performance of three recursive algorithms for fast space-variant gaussian filtering. *Real-Time Imaging, 9*, 215–228.

Valeton, J. M., & Van Norren, D. (1983). Light adaptation of primate cones : An analysis based on extracellular data. *Vision Research, 23*(12), 1539–1547.

van Hateren, J. H., & Lamb, T. D. (2006). The photocurrent response of human cones is fast and monophasic. *BMC Neuroscience, 7*(1), 34–41.

van Hateren, J. H., Rüttiger, L., Sun, H., & Lee, B. B. (2002). Processing of natural temporal stimuli by macaque retinal ganglion cells. *Journal of Neuroscience, 22*(22), 9945–9960.

Victor, J. D. (1987). The dynamics of the cat retinal X cell centre. *Journal of Physiology, 386*(1), 219–246.

Werblin, F. S., & Dowling, J. E. (1969). Organization of the retina of the mudpuppy. *Journal of Neurophysiology, 32*(3), 339–355.

Wohrer, A. (2007). *Mathematical study of a neural gain control mechanism.* Research report 6327, INRIA.

Wohrer, A. (2008a). *Model and large-scale simulator of a biological retina with contrast gain control.* PhD thesis, University of Nice Sophia-Antipolis.

Wohrer, A. (2008b). *The vertebrate retina: A functional review.* Research Report 6532, INRIA, May.